UNITED STATES
DEPARTMENT OF
COMMERCE
PUBLICATION

Design, Construction, and Testing Of a New High Accuracy Spectrophotometer

U.S.
DEPARTMENT
OF
COMMERCE

NATIONAL BUREAU OF STANDARDS

The National Bureau of Standards[1] was established by an act of Congress March 3, 1901. The Bureau's overall goal is to strengthen and advance the Nation's science and technology and facilitate their effective application for public benefit. To this end, the Bureau conducts research and provides: (1) a basis for the Nation's physical measurement system, (2) scientific and technological services for industry and government, (3) a technical basis for equity in trade, and (4) technical services to promote public safety. The Bureau consists of the Institute for Basic Standards, the Institute for Materials Research, the Institute for Applied Technology, the Center for Computer Sciences and Technology, and the Office for Information Programs.

THE INSTITUTE FOR BASIC STANDARDS provides the central basis within the United States of a complete and consistent system of physical measurement; coordinates that system with measurement systems of other nations; and furnishes essential services leading to accurate and uniform physical measurements throughout the Nation's scientific community, industry, and commerce. The Institute consists of a Center for Radiation Research, an Office of Measurement Services and the following divisions:

Applied Mathematics—Electricity—Heat—Mechanics—Optical Physics—Linac Radiation[2]—Nuclear Radiation[2]—Applied Radiation[2]—Quantum Electronics[3]—Electromagnetics[3]—Time and Frequency[3]—Laboratory Astrophysics[3]—Cryogenics[3].

THE INSTITUTE FOR MATERIALS RESEARCH conducts materials research leading to improved methods of measurement, standards, and data on the properties of well-characterized materials needed by industry, commerce, educational institutions, and Government; provides advisory and research services to other Government agencies; and develops, produces, and distributes standard reference materials. The Institute consists of the Office of Standard Reference Materials and the following divisions:

Analytical Chemistry—Polymers—Metallurgy—Inorganic Materials—Reactor Radiation—Physical Chemistry.

THE INSTITUTE FOR APPLIED TECHNOLOGY provides technical services to promote the use of available technology and to facilitate technological innovation in industry and Government; cooperates with public and private organizations leading to the development of technological standards (including mandatory safety standards), codes and methods of test; and provides technical advice and services to Government agencies upon request. The Institute also monitors NBS engineering standards activities and provides liaison between NBS and national and international engineering standards bodies. The Institute consists of the following divisions and offices:

Engineering Standards Services—Weights and Measures—Invention and Innovation—Product Evaluation Technology—Building Research—Electronic Technology—Technical Analysis—Measurement Engineering—Office of Fire Programs.

THE CENTER FOR COMPUTER SCIENCES AND TECHNOLOGY conducts research and provides technical services designed to aid Government agencies in improving cost effectiveness in the conduct of their programs through the selection, acquisition, and effective utilization of automatic data processing equipment; and serves as the principal focus within the executive branch for the development of Federal standards for automatic data processing equipment, techniques, and computer languages. The Center consists of the following offices and divisions:

Information Processing Standards—Computer Information—Computer Services—Systems Development—Information Processing Technology.

THE OFFICE FOR INFORMATION PROGRAMS promotes optimum dissemination and accessibility of scientific information generated within NBS and other agencies of the Federal Government; promotes the development of the National Standard Reference Data System and a system of information analysis centers dealing with the broader aspects of the National Measurement System; provides appropriate services to ensure that the NBS staff has optimum accessibility to the scientific information of the world, and directs the public information activities of the Bureau. The Office consists of the following organizational units:

Office of Standard Reference Data—Office of Technical Information and Publications—Library—Office of International Relations.

---

[1] Headquarters and Laboratories at Gaithersburg, Maryland, unless otherwise noted; mailing address Washington, D.C. 20234.
[2] Part of the Center for Radiation Research.
[3] Located at Boulder, Colorado 80302.

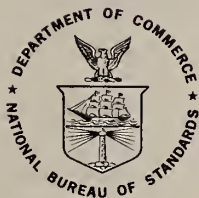# Design, Construction, and Testing Of a New High Accuracy Spectrophotometer

K. D. Mielenz and K. L. Eckerle

Institute for Basic Standards
National Bureau of Standards
Washington, D.C. 20234

t. Technical note no. 729

National Bureau of Standards Technical Note 729

Nat. Bur. Stand. (U.S.), Tech. Note 729, 60 pages (June 1972)

CODEN: NBTNAE

TABLE OF CONTENTS

DESIGN, CONSTRUCTION, AND TESTING OF A
NEW HIGH ACCURACY SPECTROPHOTOMETER

K. D. Mielenz and K. L. Eckerle

A new spectrophotometer is described which has an
accuracy of approximately 0.0001 transmittance units. The
spectrophotometer utilizes a collimated beam in the sample
area. This is accomplished by means of off-axis parabolic
mirrors in the monochromator and sample compartment. Also,
circular holes are used as entrance and exit apertures in
the monochromator. All components of this spectrophotometer
were chosen to achieve maximum accuracy. The result of
this work is a "state of the art" instrument. The instru-
ment was tested to evaluate its performance. Systematic
errors such as detector non-linearity, stray radiant energy,
and beam non-uniformity are measured. A correction for
non-linearity of the photomultiplier and electronics is
applied.

Key Words: Beam non-uniformity; circular entrance and exit
apertures; high accuracy spectrophotometer; linearity;
parabolic mirrors; stray radiant energy.

I.   Introduction

The purpose of this work was to build a spectrophotometer with
which transmittance measurements can be made accurate to within approxi-
mately 0.0001 transmittance units. This goal demands an instrument with
a minimal number of systematic errors which are as well defined as
possible and which can be measured. At the same time, the spectrophotom-
eter was designed to have flexibility in its immediate usage as well as
a capability for improving and extending its range of usefulness.

A predisperser and monochromator with wide wavelength range,
accurate wavelength settings, and narrow spectral bandpass were used.
The choice of spectral bandpass for the monochromator was dictated by
studies made by means of a commercial recording spectrophotometer and a
high dispersion Czerny-Turner grating spectrograph [1] on the resolution
necessary to measure accurately some absorption bands of a holmium oxide
glass. These measurements were assumed to exhibit a worst possible case
that would ordinarily be encountered. Figure 1 shows how the transmit-
tance of the holmium oxide glass between 440 nm and 465 nm varies with

---

[1]Figures in brackets indicate the literature references on page 24.

slit width of a commercial spectrophotometer. [2] The optical density
at the band peaks at 445.6 nm and 460 nm is plotted versus spectral
bandpass in Fig. 2. It is seen that for this case a spectral bandpass
of approximately 0.2 nm is necessary for an accurate measurement. In
view of the large dependence of transmittance on spectral bandpass, a
time exposure plate of the absorption band at 445.6 nm was made by means
of the high dispersion grating spectrograph to determine that the band
has no fine structure. [3]

Off-axis parabolic mirrors are used in the monochromator and exit
optics. Circular apertures are used as entrance and exit apertures in
the monochromator so that a well-collimated beam is provided in the sam-
ple compartment. The use of off-axis mirrors also eliminates inter-
reflections that are present in lens systems. Since the beam is colli-
mated, there is no change in focus upon insertion of a plane sample as
there is in a converging beam.

A large sample space was incorporated into the spectrophotometer
to allow for flexibility both in type of measurement and in the methods
of measurement. For example, other light beam geometries can be simu-
lated in this spectrophotometer. A detector and electronics that are
both precise and linear were used to minimize corrections necessary for
any measurement. Extensive testing described in sections II, III, and
IV below was done to characterize the performance of the instrument.

It is believed that this design; namely, the exclusive use of
off-axis mirror optics, and the placement of the samples in a collimated
beam, constitutes the optimal beam geometry for high accuracy spectro-
photometry. A detailed analysis supporting this belief may be found in
References [4] and [5].

II.   Spectrophotometer

A schematic drawing of the spectrophotometer is shown in Fig. 3.
The spectrophotometer except for the electronics and controls is con-
structed on a 122 cm by 244 cm surface plate. The optical path from the
predisperser through the photomultiplier tube is enclosed in a light
tight box. The interior of the box was coated with a flat black paint.
The optic axis was chosen to be 33 cm above the surface of the plate.
Photographs of the source side of the instrument, of the exit optics
and the detector apparatus, and of the control panel and electronics are
shown in Figures 4, 5, and 6.

A. Light Sources

Three platforms for sources of various sizes and shapes were pro-
vided. Source mounting tables having three spring loaded screws for
adjustment were constructed for a tungsten lamp (rated for 6 V and 18 A)
with a ribbon filament 14 mm long by 2 mm wide (for photometric measure-
ments) and for atomic line sources (for calibrating the wavelength
scale).

The current in the tungsten lamp is regulated by a power supply using external sensing (.01% regulation) on a special 0.1 Ω shunt rated for 50 A. A 50 Ω precision potentiometer and a 15 Ω precision potentiometer in series provide coarse and fine current controls. The reason for monitoring the voltage across the 0.1 Ω shunt is greater stability since one does not depend on the stability of a resistor internal to the power supply. Since the resistance of the shunt is constant, the system provides a constant current through the lamp. The lamp is operated in the color temperature range of 1800 °C to 2600 °C as measured by an optical pyrometer. The lamp ribbon is aligned vertically by means of a plumb line.

A 2 mW helium-neon laser was installed in the system for alignment of the optical components and of specimens to be measured. This laser is mounted in two concentric rings each of which contains three threaded screws 120° apart for leveling and adjustment as shown in Fig. 4.

B. Source Optics

The optical elements on the source side of the instrument are mounted on a 122 cm optical bench. One or more 2.5 cm diameter aluminized optical flats are necessary to divert the light beam along the optical bench. These mirrors are mounted on a support of two gimbal rings independently suspended about vertical and horizontal rotation axes. A 7.6 cm diameter aluminized mirror is placed at the end of the optical bench to divert the beam into the predisperser. This mirror is mounted on a 4-point spring-loaded device that has micrometer driven pins to rotate the mirror about two orthogonal axes. All of the mirrors can be adjusted with an angular resolution of the order of 1 arc second. The mirrors are all mounted on sturdy supports; and except for the two mirrors immediately following the laser, the mirrors are also attached to translation stages which move perpendicular (horizontally and vertically) to the light beam. The light beam is collimated over a portion of the optical bench before being focused on the predisperser. This allows convenient insertion of optical elements such as attenuators in the entrance beam. The source collimating lens is a 60 mm diameter coated glass achromat with 400 mm or 600 mm focal length depending on the size of the source. The lens which focuses an image of the source on the predisperser slit is a 200 mm focal length coated glass achromat having a diameter of 41.5 mm. Both lenses are stopped down with 2.5 cm square beveled apertures so that the light beam slightly over-fills the grating of the monochromator.

C. Intensity Attenuators

The tungsten source intensity reaching the detector can be varied by changing the current in the lamp or by rotating an inconel coated neutral density wedge. The neutral density wedge is 15.2 cm in diameter, varies in optical density to 2.0, and is rotated remotely by means of a stepping motor attached to the circular wedge. It is used primarily to attenuate the beam for linearity measurements rather than for transmittance measurements since it is placed after the collimating lens and

introduces additional inhomogeneity in the beam. It is also possible
to replace the neutral density wedge by a rotating Glan-Thompson placed
in the optical path as shown in Fig. 3 and discussed in Section II.G.

D. Predisperser

The predisperser is an Ebert quartz prism instrument with a 500 μm
entrance slit. It has 15.2 cm focal length collimating and focusing
mirrors and a horizontal aperture ratio of f/6. The wavelength range of
this instrument is from 180 nm to 1.7 μm. The wavelength driveshaft of
the predisperser is coupled to the monochromator wavelength drive to
synchronize their movements.[6]

E. Monochromator

The monochromator is a 1 m Czerny-Turner system with effective
aperture of f/8.7. The manufacturer states that its useful wavelength
range is from less than 200 nm to greater than 30 μm if the appropriate
grating is chosen. The grating presently in use is a plane grating 102 mm
by 102 mm. The grating has 1200 grooves per mm, is blazed at 500 nm,
and has a useful wavelength range from approximately 185 nm to 1.3 μm.
The monochromator has a linear dispersion of 0.833 nm/mm.

The monochromator collimating and focusing mirrors are off-axis
parabolas. The surfaces of the mirrors were specified to be paraboloidal
to within 0.1 fringe in green light and to be free of zones. These
mirrors travel along a rail in the base and are both driven by micrometer
screws.

The entrance and exit apertures of the monochromator can each be
chosen from a selection of 4 circular holes having diameters of 250, 500,
750, or 1000 μm. These apertures can be rotated alternately into posi-
tion. The exit aperture thus approximates a point source with band-
pass of about 0.2, 0.4, 0.6 or 0.8 nm. This was checked by scanning the
atomic line of the HgI spectrum at 546.07 nm. At the same time, the
deviation from concentricity of the four apertures was determined.
Repeatability of switching a particular aperture into place is within the
uncertainty of the measurements. The exit apertures were blackened
chemically so that their specular reflectance is approximately 7%.

The wavelength dial of this instrument can be set to a precision
of 0.01 nm, which is the least count of the output vernier. This dial is
calibrated using atomic lines of HeI, NeI, and HgI with peaks
throughout the wavelength range of 380 nm to 850 nm. The results are
repeatable to 0.01 nm. It was judged from the resulting calibration
curve (see Figure 7 for the data for the 250 μm apertures) that at any
arbitrary wavelength in the above range, the dial can be corrected
accurately to 0.02 nm. It was verified that wavelength corrections for
other size pinholes differed by a constant amount from the corrections
for the 250 μm pinholes. The temperature coefficient for the wavelength
correction is approximately -0.01 nm for a 1 °C increase in temperature.

Since the light path through the monochromator is opposite to that for which the monochromator was designed, [6] several changes in the baffles were necessary to eliminate possible sources of stray radiant energy in this instrument. The original entrance slit baffle was placed at the new entrance slit. An identical baffle (with the beveled edge on the opposite side) was installed at the new exit slit. Since the oversize collimating mirror (original focusing mirror oversize to accommodate a camera attachment) is now present, it was stopped down with a mask. A baffle attached to the cover approximately midway between the entrance slit and the new collimating mirror was enlarged since the collimating mirror was stopped down. Since the interior mounting platform of the monochromator was highly reflective, it was covered with a black velvet cloth.

F. Sample Compartment Optics and Light Beam

After the light beam leaves the monochromator, a 2.5 cm diameter optical flat diverts the beam into an off-axis parabolic mirror as shown schematically in Figure 8. This produces a 20 mm square collimated light beam. At the other end of a 122 cm precision optical bench, the light beam is collected by another off-axis parabolic mirror and is diverted into an averaging sphere by another optical flat. The optical flats each have a beveled edge to allow the light beam to be unobstructed. They are attached to rods and are mounted off center on three point spring loaded supports. The angles of incidence (50°) on these flats are close to the angle of restored polarization so that these flats will not significantly depolarize the light. The parabolic mirrors have a 3.4 cm diameter and 195 mm focal length. They are off-axis by an angle of 8.5° and are free of zones. The optic axes of the two parabolic mirrors are on opposite sides of the optical bench i.e., the parabolic mirrors are mounted in a "z" geometry.

The parabolic mirrors are mounted in gimbal supports similar to those discussed above which are in turn mounted to two micrometer driven translation stages which give motion in two directions parallel and perpendicular to the light beam. The translation stages are in turn attached to a 5.1 cm diameter cylinder which slides in another hollow 7.6 cm diameter cylinder which is attached to the optical bench to give a vertical adjustment.

The parabolic mirrors were tested individually and together in the "z" geometry by means of a shearing interferometer [7] as shown in Fig. 9a,b. The laser (632.8 nm) and microscope objective provided a point source of light at the focal point of the mirrors. The angle between the principal axis of the incident light and the reflected light was 8.5°. The high quality 192 mm focal length lens was used when the mirrors were tested individually. Pictures of the resulting fringe patterns were taken and were evaluated perpendicular to the fringes at increments of the shear. The deviation from straightness of the fringes was measured at the center of the mirrors, and also at half their radius on either side, both with the shear horizontal and vertical. No significant difference was obtained from measuring the mirrors individually and

5

together in the "z" geometry. The average deviation from a spherical wave front was found to be approximately 2/5 of a fringe for the horizontal shear and 1/5 of a fringe for the vertical shear.

The parabolic mirrors are aligned from geometrical drawings as a first step. The fine alignment of the first parabolic mirror is done by moving a 5 mm diameter aperture from one end of the optical bench to the other adjusting the mirror until the intensity along the optical bench remained constant.

Measurements were also made of the uniformity of this collimated beam. A 5 mm diameter aperture was scanned across the beam in a vertical and horizontal direction at different wavelengths. The results can be seen in Figs. 10 and 11. It is seen that in the vertical direction the signal is constant to ± 0.1%. In the horizontal direction the light beam has a gradient which was found to be increasing with wavelength. This gradient is attributed to a variation of blaze angle across the grating since the diamond head which cuts the grooves wears out as preparation of the master grating is made.

The non-uniformity of the beam has no effect on the measured transmittance of a homogeneous filter. If the filter is not homogeneous, the corresponding measurement error is, according to Eq. A6 in Appendix A,

$$\Delta T = \overline{T}_A - \overline{T} = \frac{1}{12} \overline{T} \alpha\beta x^2 \quad . \tag{1}$$

This is negligibly small even if filter and beam are quite inhomogeneous. For example, if the beam non-uniformity is as large as 10% over a 10 mm area (as in the worst case shown in Fig. 11), and if the filter transmittance varies by 1% over this area, then $\alpha = 10^{-3}$/mm, $\beta = 10^{-2}$/mm, $x = 10$ mm, and

$$\Delta T/\overline{T} = 8 \times 10^{-5} \quad . \tag{2}$$

The error is eliminated altogether if the mean is taken of the two transmittance measurements before and after the filter is rotated by 180° so that its gradient is reversed. The above numerical example indicates that these two measurements would differ only if the filter is grossly inhomogeneous (e.g.; by more than 1% over a 10 mm area). In such extreme cases, the average transmittance $\overline{T}$ is hardly a meaningful quantity, and the filter should be mapped by measuring T(x) with apertures of small width. Because of the dependence of ΔT on x^2 in Eq. 1, beam non-uniformity will not noticeably affect such measurements.

G. Polarizer

A Glan-Thompson prism in a rotatable mount is placed in the beam to produce a defined state of polarization. This is necessary since it is

6

well known that tungsten sources and grating monochromators produce polarized light whose state of polarization varies with wavelength. An example of the polarization of the beam is shown in Fig. 12 (polar plot with an arbitrary scale of the transmittance of a sheet polarizer) at 564 nm and computed to be 23%. Zero degrees denotes the orientation of the polarizer at which the electric vector is perpendicular to the grating grooves. The presence of Wood's anomalies which are due to the grating further complicates the state of polarization of the beam. The polarization of the same models predisperser and monochromator illuminated with a xenon source as measured at the manufacturer's plant is shown in Fig. 13 for the wavelength range of 410 nm to 600 nm. The degree of polarization is expressed as $T_{90°}/T_{0°}$ where $T_{90°}$ and $T_{0°}$ are the transmittances of a sheet polarizer with the electric vector parallel and perpendicular to the grating grooves.

The Glan-Thompson prism can be placed in the collimated beam on the source side of the instrument or between the two off-axis parabolas in the sample compartment. If the prism is placed on the source side, it must be verified that the monochromator does not produce partially polarized light for the wavelength at which the measurements are made. It was found for several wavelengths at which measurements were performed that the prism could be put on the source side as long as the electric vector was either parallel or perpendicular to the grating grooves. If the prism is placed in the sample compartment, it must be tilted with respect to the optic axis to avoid inter-reflections between the prism and the sample. However, the prism can not be tilted too much since it polarizes for only small angles of incidence.

H. Double Aperture Linearity Device

A two aperture linearity tester with 5 mm diameter beveled holes whose centers are separated by 10 mm was constructed and can be placed in the sample compartment (see Fig. 14). These apertures are opened and closed by two cylinders driven by compressed nitrogen. These cylinders are opened and closed by two-way gas valves in which the direction of flow is controlled by two solenoids located remote to the detector. The linearity test is automated by means of a data acquisition and control system as discussed below in Section IV.

I. Sample Holders

Two sample holders were constructed utilizing four-position Geneva mechanisms--thus providing for 3 samples plus 1 clear space. These Geneva mechanisms are driven by reversible synchronous motors which rotate at 4 rpm and have a torque of 8600 gcm. When the motor rotates 360°, the Geneva mechanism rotates 90°. The holders have adjustments so that the filters can be oriented relative to the beam in a normal mode or tilted slightly. The filters can be scanned across the beam horizontally or vertically. Behind the sample holders, a compressed nitrogen operated remotely controlled shutter was placed to determine the "zero" level of the electronics.

J. Averaging Sphere

After the light is collected by the final parabolic mirror, it passes into a six inch diameter averaging sphere whose interior is coated with a 1/8 inch layer of pressed barium sulfate. This sphere was carefully constructed so that no first reflections from the sphere wall can reach the photocathode of the detector whose housing is attached to the sphere. Another compressed nitrogen operated, remotely controlled shutter was constructed between the sphere and the photomultiplier tube. The design of the sphere was dictated by the size of the photocathode (masked down to 44 mm diameter) and by questions of efficiency. The light beam is focused at the entrance port of the sphere as seen in Fig. 15. The efficiency of the sphere can be shown (see Appendix B) to be:

$$\varepsilon = \frac{(A'A_D/\pi e^2 A_s)\ r^2}{1 - r[1 - (A + A')/A_s]} \tag{3}$$

In our case, $A_D \approx 14.8\ cm^2$, $A' \approx 19.4\ cm^2$, $A_s \approx 645\ cm^2$, $A \approx 2.58\ cm^2$, $r \approx .98$ and $e \approx 3.8\ cm$; so that the calculated efficiency is found to be $\approx 20\%$.

K. Detector

The photomultiplier is an 11 stage end-on device with an S-20 surface. The dynode chain is a linear potted resistor chain with a zener diode between the cathode and the first dynode which was purchased from the manufacturer of the detector. The high voltage power supply is voltage regulated to .001%.

L. Anode Current Measuring System

The anode current is measured by means of a current to frequency converter. This instrument together with a high accuracy counter (used with 10 second integration time) was found to be linear to .01% or better by measuring currents produced in precision resistors by a calibrated voltage source (.01% accuracy). By this same method, the current to frequency converter and counter were found to be precise to at least 1 part in 45,000 on the current ranges normally used. Low noise cable is used.

The electrical output of the converter is not a true frequency; the translation of the current input is events per unit time. The waveform at the output is a series of constant width rectangular pulses whose number per unit time is a linear function of the input current to the converter. The pulse rate (number of pulses per second at any instant) is not necessarily constant for a fixed value of input current, for in the presence of input noise the output pulse rate will be random over a short interval. Yet, it will yield the correct pulse count during the relatively long 10 second measuring period of integration since the

8

random variations will be averaged.

The constructed converter is basically identical to the circuit
described by Taylor [8]. Some component changes were made in order to
enable the circuit to function in the desired manner--mostly at the
"single-shot" stage following the clock oscillator and the "flip-flop"
stage following the gate. Additional circuit components were added at
the input of the operational amplifier consisting of a fuse and pair of
low-leakage shunt diodes for the purpose of protecting the operational
amplifier from damaging overload by excessive excitation from the photo-
multiplier tube. A low pass filter was also added to the input line
for removing higher frequency noise components that may be present in the
input signal which could interfere with the subsequent gating function.
A shunt diode was added to the output line of the operational amplifier
stage for the purpose of negative clipping at the base of the transistor
stage driven by the operational amplifier thus keeping its emitter to
base voltage below the maximum rating.

The use of an event counter with a precise measuring gate time in
conjunction with the converter yields an input-output transfer expression
having the following equation for noise rejection:

$$\text{rejection in dB} = 20 \log(\pi F_N T_G) - 20 \log(\sin \pi F_N T_G) \tag{4}$$

where F_N is the noise frequency and T_G is the integrating gate time with-
in the counter. The first term is recognized as the attenuation charac-
teristic of a single section low pass filter. The second term shows
additional notches of infinite rejection for periodic noise whose fre-
quency, F_N, represents multiple fractions of the period T_G. Experience
shows that it is the low frequency noise that precludes the precise
measurement of low level signals in the area of use by the converter.
For example: considering a noise frequency F_N of 1 Hz and a gating time
T_G of 10 seconds, the achievable attenuation with the converter com-
puted from the first term of the above expression is 30 dB on a voltage
or current basis. It is difficult to approach this performance with
either lump-passive or with active low-pass filters. The problem with
passive low-pass filters is the wasted time in waiting for the output
to reach final value; it takes 9.2 RC time constants to reach 0.01% of
the final value. Active low pass filters can exhibit fast response time
for an equivalent attenuation but their settling time precision is not
compatible in general with the desired 0.01% figure.

The gated-integrator feature of the described converter has a
fixed reading accuracy figure that is dictated by the precision of the
gating time which can be a part per million or better in most counters
while the accuracy figure with a low pass filter is related to the time
in reaching final value. Carefully designed multi-section low-pass
filters can shorten the response time while preserving the desired
attenuation.

The dark current from the photomultiplier tube is shown in Fig. 16 as a function of dynode voltage. This dark current was measured by closing the shutter between the sphere and the detector. No measureable stray light was detected upon opening this shutter.

M. Data Acquisition and Data Processing

Data are obtained by means of a data acquisition and control system consisting of a teletypewriter, logic circuits, and four electrical switches. The control system has start and stop codes, codes for recording data, and codes for sequentially actuating the electrical switches. These can be programmed by means of a punched-paper tape. When the counter finishes its integration, it signals the acquisition system to record a datum point on punched-paper tape. For measurements which are not yet automated, the count is initiated by pushing a start botton. For automated measurements, the counter is set to repetitively count for ten seconds after waiting ten seconds. The switches are used to open and close apertures and shutters automatically for linearity measurements by means of a network of diodes and relays. The teletypewriter is also used as a computer terminal by means of an acoustic coupler to process the punched-paper tape.

N. Equipment

The more important pieces of apparatus, their model numbers and manufacturers are listed in Table I. [9]

III. Alignments

A. Monochromator Alignment

It was established by means of a Twyman-Green interferometer that the surface of the grating was flat to approximately 2/5 fringe in both the directions parallel and perpendicular to the grooves (see Fig. 17). An autocollimator, focused on infinity for the observer's eye, was used to align the parabolic mirrors as shown in Fig. 18 using a Hg lamp focused on the entrance aperture. The light reflected from each mirror individually via the grating in the zero order was observed and the mirror under test was adjusted until the light reaching the autocollimator was parallel. However, since the grating had been found to deviate from flatness, this was not the final setting since the parallelism of the light was influenced by the grating. It was judged, however, that the relative separation of the settings for the two mirrors should be correct. Thus, the two mirrors were moved by fixed amounts in the same direction to correct for abberations of the grating.

A fine adjustment can be made with the Foucault test. The direction in which the darkness crossed the grating was observed for a given direction of rotation of the wavelength screw as observed at the exit slit. Then, the mirrors could be adjusted (always moving them both in the same direction and by the same distance). The distance moved was

always halved between observations, thus converging on the true posi-
tion. These settings were checked with the Hg lamp for the zero order,
for the first order green line (546.07 nm), and for the second order
green line. Finally the Hg lamp was focused on the exit slit, and the
Foucault test was repeated at the entrance aperture.

B. Alignment of Optics

The optical system is aligned in the following manner. The laser
beam is adjusted until its path is 33 cm above the surface plate before
and after each reflection from a mirror and parallel to the optical
bench on the source side of the instrument. Lenses can then be intro-
duced into the beam and adjusted so that they do not deflect the laser
beam. The monochromator's three leveling screws are then turned until
the laser light hits the center of the monochromator collimating and
focusing mirrors and the grating which are defined by masks with circular
holes in the centers. After the light leaves the monochromator, it is
33 cm above the surface plate, hits the centers of the parabolic mirrors,
and is parallel to the optical bench on the exit side of the monochro-
mator. The positions of the optical flats and the parabolic mirrors are
determined by the distances measured from a geometrical drawing of the
light path accounting for the 8.5° off-axis parabolic mirrors and the
20 mm by 20 mm size of the beam when the grating is fully illuminated.
The position of the averaging sphere is determined from a geometrical
drawing.

IV.   Performance and Operation of Spectrophotometer

A. Measurement of Stray Radiant Energy

Stray radiant energy which passes through the predisperser and
monochromator was measured by three independent methods. The largest
apertures were used for these tests (1 mm diameter) giving the worst
possible amount of stray radiant energy.

The first test follows the ASTM method E387 [10] using a .005%
methylene blue aqueous solution. A 1 cm cell of this solution was
measured on a commerical recording spectrophotometer. The solution
transmits the yellow and blue light as well as some red and also has a
strong absorption band at 660 nm. A 1 cm cell of this solution was
measured at 660 nm on the spectrophotometer under discussion here and the
percentage of scattered light plus the transmission of the solution was
found to be 1.4×10^{-4} which is of the same order of magnitude as
measured on the commercial spectrophotometer by placing two screens in
its reference beam. It was therefore judged that a 2 cm solution would
have negligible transmission at 660 nm, and the percentage of stray
radiant energy as measured from a 2 cm cell was found to be about 5
parts in 100,000.

The second method employed the measurement of two selenium red
glasses each of which had a transmittance of less than 1×10^{-4} at

400 nm, 450 nm, and 500 nm as measured on the commercial recording spectrophotometer. The transmittance measured on the high accuracy spectrophotometer at 400 nm, 450 nm, and 500 nm for one selenium red glass and two selenium glasses was found to be:

Wavelength (nm)	Transmittance of one glass	Transmittance of two glasses
400	1.4×10^{-6}	1.8×10^{-6}
450	1.5×10^{-6}	1.4×10^{-6}
500	5.3×10^{-6}	3.0×10^{-6}

This indicates stray radiant energy of a few parts in one million from the red portion of the spectrum.

Finally, the intensity of the helium-neon laser light whose spatial coherence had been reduced by a beam expander and an oscillating ground glass was measured at 632.8 nm. Fractions of this value were measured at other wavelengths giving an indication of the stray radiant energy. Typical values obtained at several wavelengths are listed below:

Wavelength (nm)	Fraction of Stray Radiant Energy
400	2.3×10^{-6}
500	2.1×10^{-6}
600	6.3×10^{-6}
630	69.5×10^{-6}
700	8.4×10^{-6}

B. Double-Aperture Linearity Testing

The purpose of this test is to determine a linearity correction, ΔT, which can be applied to the measured transmittance, T_a, such that the true transmittance, T, is:

$$T = T_a + \Delta T \tag{5}$$

Since a complete discussion of linearity testing using a double aperture has been published elsewhere [11], this description will deal only with practical details.

Studies were made of the observed signal as a function of time. Three typical cases are shown in Fig. 19. In all cases, the drift was approximately linear over a 30 minute time interval. The slope of the curve was not always negative.

Three quantities are measured in the double aperture method: I(A), the intensity reading for aperture A alone; I(B), the reading for aperture B; and I(A+B), the reading for both apertures at once. These determine a quantity σ(A,B) defined by

$$1 + \sigma(A,B) = \frac{I(A+B)}{I(A)+I(B)} \qquad (6)$$

If σ(A,B) is not zero, the system is not linear.

Defining φ as the total flux when both apertures are open, σ(φ) is determined in the following manner. The data acquisition and control system is programmed to actuate the valves operating the shutters such that 27 readings, 0, A+B, 0, A, 0, B, 0, A+B, 0, B, 0, A, 0, A+B, 0, A, 0, B, 0, A+B, 0, B, 0, A, 0, A+B, 0 are effected at 20 second intervals and recorded on punched-paper tape. The signal counter initiates a count after a 10 second interval, counts for 10 seconds, and then activates the data acquisition and control system which punches a datum point on paper tape and then opens or closes the appropriate shutters after which the cycle is repeated.

Here, "0" is a dark-current reading; and "A", "B", and "A+B" are the readings obtained with either or both apertures open. A computer program was written to perform the following calculations. The dark currents on both sides of "A", "B", or "A+B" are averaged and subtracted from these readings, yielding a sequence of 13 adjusted signal currents,

$$I_1(A+B), \; I_1(A), \; I_1(B), \; I_2(A+B), \; I_2(B), \ldots I_4(A), \; I_5(A+B) \quad .$$

The averages $\overline{I(A)}$, $\overline{I(B)}$, and $\overline{I(A+B)}$ are then used to compute

$$\sigma(\phi) = \overline{I(A+B)}/[\overline{I(A)} + \overline{I(B)}] - 1 \quad , \qquad (7)$$

as defined by Eq. 6. In order to determine the standard deviation of this value of σ, the 13 quantities

$$Y_i = \frac{I_1(A+B)}{\overline{I(A+B)}} , \; \frac{I_1(A)}{\overline{I(A)}} , \; \frac{I_1(B)}{\overline{I(B)}} , \; \frac{I_2(A+B)}{\overline{I(A+B)}} , \; \frac{I_2(B)}{\overline{I(B)}} , \ldots \frac{I_4(A)}{\overline{I(A)}} , \; \frac{I_5(A+B)}{\overline{I(A+B)}} \qquad (8)$$

are fitted by least squares to a linear function of time,

$$\overline{Y_i} = p + qt_i \quad , \tag{9}$$

where q is the average drift for 40 seconds. Typical values calculated for q ranged in magnitude from 0.001% to 0.008%.

The standard errors in I(A), I(B), and I(A+B) are given by

$$dI(A) = \left(\frac{[I_1(A) - \overline{I(A)}(p+2q)]^2 + [I_2(A) - \overline{I(A)}(p+6q)]^2 + \dots}{12} \right)^{1/2} \tag{10}$$

$$dI(B) = \left(\frac{[I_1(B) - \overline{I(B)}(p+3q)]^2 + [I_2(B) - \overline{I(B)}(p+5q)]^2 + \dots}{12} \right)^{1/2} \tag{11}$$

and

$$dI(A+B) = \left(\frac{[I_1(A+B) - \overline{I(A+B)}(p+q)]^2 + [I_2(A+B) - \overline{I(A+B)}(p+4q)]^2 + \dots}{20} \right)^{1/2} \tag{12}$$

The uncertainty in σ is then given by equation (20) in reference [11] as

$$[d\sigma(\phi)]^2 = \frac{1}{[\overline{I(A)} + \overline{I(B)}]^2} \left\{ [1 + \sigma(\phi)]^2 \ [dI(A)^2 + dI(B)^2] + dI(A+B)^2 \right\} \tag{13}$$

Since σ is a small quantity, the statistical fluctuations must be sufficiently small to make a meaningful measurement. The quantity which was used as a criterion for a valid measurement was:

$$\frac{dI}{I} \approx dY_i = \left[\sum_{i=1}^{13} \frac{Y_i - p - qt_i}{12} \right]^{1/2} \quad . \tag{14}$$

This quantity is plotted in Fig. 20 versus I. As indicated by the solid line, the relationship between dI and I is, approximately

$$\frac{dI}{I} = \begin{cases} \sqrt{10/I} \times 10^{-7} & \text{if } I < 10^{-7} \text{ A} \quad (15a) \\ \\ 10^{-4} & \text{if } I > 10^{-7} \text{ A} \quad (15b) \end{cases}$$

14

The signal-to-noise ratio, I/dI, being proportional to $\sqrt{I}$ for the small anode currents below 10^{-7} A suggests that, in this region, the flux measurements are limited by photomultiplier shot noise. For a photomultiplier with linear dynode chain the theoretical expression for the shot noise, due to photon noise of the incident flux and noise contributions from the photocathode and the dynode chain, is [12]

$$\frac{I}{dI} = \sqrt{\frac{n\tau(\delta - 1)}{\delta^k + 1}} = \sqrt{\frac{I\tau(\delta - 1)}{q\delta^k + 1}} \quad , \tag{16}$$

where $n = I/q$ is the average arrival rate of electrons at the anode, $q = 1.6 \times 10^{-19}$ As is the electron charge, τ is the integrating time, δ is the gain per dynode, and k is the number of dynodes. In our case $\tau = 10$ s and $k = 11$, so that eqs. (15a) and (16) may be identified with each other if $\delta^{12}/(\delta - 1) \approx 6 \times 10^6$, or $\delta \approx 4$. Since this is the correct order of magnitude [13] for δ, the measured signal uncertainty dI for $I < 10^{-7}$ A may indeed be interpreted as photomultiplier shot noise. The limiting value (15b) of dI for signal currents $I > 10^{-7}$ A is attributed to lamp noise.

The above method only defines σ for one value of the flux ϕ. A plot was made of σ versus I for values of ϕ yielding anode currents ranging from 3×10^{-6} to 6×10^{-9} A as shown in Fig. 21. These measurements were made with high voltages on the photomultiplier tube of 750V, 850V, and 950V. It was found that the non-linearity was independent of which of these three voltages was used; but rather, the non-linearity depended on the anode current.

It is shown in reference [11] that it is possible to measure $\sigma(T\phi)$ for evenly distributed values of T rather than attenuating by factors of 2 as is customary. To measure $\sigma(T\phi)$ versus T, a lamp current is chosen so that the unattenuated flux ϕ through both apertures corresponds to the 100% point of the transmittance scale. After $\sigma(\phi)$ has been measured as described above, the incident flux is attenuated in four 20% steps, $\sigma(T\phi)$ is measured for T = 0.8, 0.6, 0.4, and 0.2. This series of measurements is then repeated four times.

An example of the results is shown in Fig. 22. In all cases, the dependence of σ on T could be represented in the form of a parabola,

$$\sigma(T\phi) = aT + bT^2 \quad . \tag{17}$$

A statistical analysis showed that the residuals had no pattern suggesting higher order terms. As shown in Eq. (19) of reference [11], the non-linearity correction ΔT is then given by

15

$$\Delta T = \frac{2aT_a(1 - T_a) + \frac{4}{3}(a^2 + b)T_a(1 - T_a)^2}{1 + 2a + \frac{4}{3}(a^2 + b)} \qquad (18)$$

An analysis was done using T_a, $\sigma(T\phi)$, and $d\sigma(T\phi)$ to compute ΔT and its standard error as a function T [14]. The individual data for σ were weighted by the reciprocal square of the $d\sigma$ of Eq. 13. The standard error for ΔT was computed from a propagation of error formula based on Eq. 18. A typical curve of ΔT versus T is shown in Fig. 23 with the shaded area denoting ± one standard deviation. The non-linearity correction, ΔT, can be determined to a high degree of precision (see Table II). The linearity correction was found to be independent of source polarization, free from interference errors, but slightly dependent on wavelength. Columns headed 0° and 90° in Table III show that for the electric vector perpendicular and parallel to the grating grooves, there is no difference in linearity to 1 part in 100,000. The column headed by ± 45° shows that for two polarizers at the double apertures at 90° with respect to each other and at 45° with respect to another polarizer, there is no significant change in linearity as compared to columns 2 and 3. This shows that the measurements are not biased by interference. However, comparison of the columns headed by 525 nm, and with the columns headed by 400 nm and 750 nm shows a slight dependence on wavelength. This difference was verified by a statistical analysis of the data [14].

C. Transmittance Measurements

The random error dT_a of the measured transmittance T_a is given by

$$\frac{dT_a}{T_a} = \sqrt{\left[\frac{dI(T_a\phi)}{I(T\phi)}\right]^2 + \left[\frac{dI(\phi)}{I(\phi)}\right]^2} \qquad , \qquad (19)$$

where ϕ is the radiant flux corresponding to the 100% point of the transmittance scale. This relationship can be used, together with the values of dI/I from Eqs. (15a,b) to calculate dT_a versus $I(\phi)$ for given values of T_a. A family of curves thus generated is shown in Fig. 24. The error is largest if $T_a = 1$, in which case

$$dT_a \leq \sqrt{2} \times 10^{-4} \quad \text{if} \quad I(\phi) \geq 10^{-7} \text{ A}. \qquad (20)$$

Thus, a single measurement of $I(T_a\phi)$ and $I(\phi)$ may be expected to give T_a to within approximately 10^{-4} transmittance units as long as the operating conditions of the spectrophotometer are chosen such that the anode current corresponding to 100% transmittance is not smaller than 10^{-7} A. We chose 3×10^{-7} A as the normal 100% signal current for the spectrophotometer with a photomultiplier voltage of 850V.

16

Measurements based on a series of repeated readings, such as listed above, will then be reproducible to within a few 0.00001 transmittance units. This expectation was verified directly, when separate transmission measurements of neutral-density glass filters with nominal transmittances of 0.1, 0.2, and 0.3 were found to be repeatable to ± 0.00004 (see Section V). Transmittance measurements are made in a defined polarization, e.g., either with the electric vector parallel or perpendicular to the grating grooves.

The filter wheel accommodates three filters plus a clear space so that either one, two, or three filters may be measured in a given run. We will discuss the procedure for a three filter measurement from which it should be obvious how one would measure one or two filters. Since it was shown in Section IV.B above that the drift of the system is predominantly linear, we perform a series of measurements designed to eleminate the linear drift as in the case of the linearity test. We chose to record data for 0, F_0, 0, F_1, 0, F_2, 0, F_3, 0, F_0, 0, F_3, 0, F_2, 0, F_1, 0, F_0, 0, F_1, 0, F_2, 0, F_3, 0, F_0, 0, F_3, 0, F_2, 0, F_1, 0, F_0 where F_0, F_1, F_2, F_3 are the signals for the fluxes of a clear space, filter 1, filter 2, and filter 3; and "0" is the dark current reading. Since the filter wheel is controlled remotely and the driving motor is reversible, this sequence of measurements was achievable easily with the time elapsed between F_0 and F_1, and F_1 and F_2, etc. being 1 minute. These measurements are not yet automated so that the counter had to be activated at fixed intervals after which it integrated over a ten second interval. However, after terminating its integration, the counter signaled the control-log to record a datum point on a punched-paper tape.

A computer program was written to analyze the data in a manner similar to that for the linearity test. The dark current on both sides of "F_0", "F_1", "F_2", are averaged and subtracted from these readings, yielding a sequence of 17 adjusted signal currents, I_{01}, I_{11}, I_{21}, I_{31}, I_{02}, I_{32}, I_{22}, ..., I_{14}, I_{05}. The averages $\overline{I_0}$, $\overline{I_1}$, $\overline{I_2}$, and $\overline{I_3}$ are then used to compute the transmittance

$$T_j = \frac{\overline{I_j}}{\overline{I_o}} \quad . \tag{21}$$

for filter j. The set of 17 Y_i

$$Y_i = \frac{I_{01}}{\overline{I_0}} , \frac{I_{11}}{\overline{I_1}}, \frac{I_{21}}{\overline{I_2}} , \frac{I_{31}}{\overline{I_3}} , \cdots \frac{I_{14}}{\overline{I_1}} , \frac{I_{05}}{\overline{I_0}} \tag{22}$$

may be fitted to a straight line, and the coefficient of variation of the data may be calculated. A typical value for this parameter is found to be 0.02%.

Again assuming

$$\overline{Y_i} = p + qt_i \qquad (23)$$

the standard errors, dI_0, dI_1, dI_2, and dI_3 may be calculated. Then, the standard error in the transmittance measurement for filter j is

$$dT_j = T_j \left[\left(\frac{dI_0}{I_0} \right)^2 + \left(\frac{dI_j}{I_j} \right)^2 \right]^{1/2} . \qquad (24)$$

This quantity was as large as .007% for a 60% filter; but for T_j less than 50%, dT_j was typically less than .004%.

The computer program also calculates a linearity correction $\Delta T(\lambda, T)$ by a numerical interpolation formula,

$$\Delta T(\lambda, T) = \Delta T(\lambda_0, T) \left[1 + f(\lambda - \lambda_0) + g(\lambda - \lambda_0)^2 \right] \qquad (25)$$

using values of f and g in Eq. (25) computed from the linearity data at 400 nm, 525 nm, and 750 nm.

V. Results of a Specific Test

Three filters were obtained from Dr. Radu Mavrodineanu from sets which are certified and issued as Standard Reference Material 930, as measured with his spectrophotometer [15].

The three filters labeled with their approximate transmittances (10%, 20%, and 30%) were measured on our high accuracy spectrophotometer. The spectral bandpass for these measurements was approximately 0.8 nm, and the temperature was 23.0 °C ± 0.5 °C. The filters were aligned normal to the light beam by means of the alignment laser. Three sets of measurements at the wavelengths for which the glass filters are certified were made in collimated light averaging over an area of approximately 2 mm by 12 mm. These measurements were made using polarized light with the angle of polarization parallel or perpendicular to the grating grooves. A measurement with parallel or perpendicular polarization consisted of 4 determinations as described above. The average value of parallel and perpendicular polarization is reported in Tables IV, V, and VI as Runs 1, 2, and 3. The difference between the values furnished by Dr. Mavrodineanu and our values are listed in Tables IV, V, and VI as well as the difference between values for the parallel and perpendicular polarizations.

Between Run 1 and Run 2, a realignment of the optics was made so that the area of the filter measured in Runs 1 and 2 were not quite the same indicating that the filters (especially the one designated 10%) are not uniform. The agreement between Runs 2 and 3, when no changes were made, attest to the reproducibility of our instrument (approximately ± 0.00004 transmittance units).

Since there is an indication of non-uniformity, the filters were moved across the 2 mm wide aperture in 1 mm steps scanning a 4 mm wide section of the filters for parallel polarization at 635 nm in collimated light. The results are listed in Table VII.

All values of transmittance listed in the Tables have been corrected for non-linearity of the instrument as a function of wavelength.

It should be noted that non-uniformity is not peculiar to these filters. Three neutral filters of another type were measured; and they exhibited similar non-uniformity.

VI. Appendices

A. Discussion of Beam Non-Uniformity

Let $T(x)$ be the transmittance of a filter area element between x and $x + dx$, and let $\phi(x)$ be the radiant flux incident upon it. Then the measured apparent transmittance of a filter area of width x,

$$\overline{T}_A = \frac{\int_{-\frac{1}{2}x}^{\frac{1}{2}x} dx\, T(x)\, \phi(x)}{\int_{-\frac{1}{2}x}^{\frac{1}{2}x} dx\, \phi(x)} \qquad (A1)$$

is different from the true transmittance,

$$\overline{T} = \int_{-\frac{1}{2}x}^{\frac{1}{2}x} dx\, T(x) \qquad , \qquad (A2)$$

provided that both filter and beam are non-uniform.

If we assume linear gradients in $T(x)$ and $\phi(x)$ such that

19

$$T(x) = \overline{T}(1 + \alpha x) \quad , \tag{A3}$$

$$\phi(x) = \phi(1 + \beta x) \quad , \tag{A4}$$

then

$$\overline{T}_A = \overline{T} \, \frac{\displaystyle\int_{-\frac{1}{2}x}^{\frac{1}{2}x} dx[1 + (\alpha + \beta)x + \alpha\beta x^2]}{\displaystyle\int_{-\frac{1}{2}x}^{\frac{1}{2}x} dx(1 + \beta x)} \tag{A5}$$

$$= \overline{T}\left(1 + \frac{1}{12}\alpha\beta x^2\right) \quad . \tag{A6}$$

which is used in Section II.F. above.

B. Derivation of Efficiency of Averaging Sphere

The efficiency, ε, of the averaging sphere will be defined as the ratio of the flux incident upon the detector, ϕ', to the flux entering the sphere, ϕ;

$$\varepsilon = \phi'/\phi \tag{B1}$$

A number of parameters will be defined as in Fig. 25. Let

d = inside diameter of the sphere
$A_S = \pi d^2$ = total inside area of the sphere
e = distance separating sphere and detector
A_D = photosensitive area of the detector
A = area of entrance port
A' = area of exit port
A_I = directly illuminated area of sphere
A_V = area of sphere viewed by the detector
Ω = solid angle subtended at detector by A' or A_V

With L as the diffuse radiance (W/m^2/sr) of the uniformly illuminated sphere wall, the flux from a surface element dA_V of the sphere wall onto a surface element dA_D of the detector is

$$d\phi' = LdA_D \, \frac{dA_V}{z^2} \tag{B2}$$

20

where Z is the distance between dA_V and dA_D as shown in Fig. 25. Generally, Z is a complicated function of sphere geometry; but for the present purpose, we can replace Z by its approximate value $(d + e)$. Then the total flux into the detector is

$$\phi' = \frac{L}{(d + e)^2} \int_0^{A_D} \int_0^{A_V} dA_D dA_V \tag{B3}$$

$$= LA_D \frac{A_V}{(d + e)^2} \tag{B4}$$

According to Fig. 25, provided that $\ell \neq 0$,

$$\frac{A_V}{(d + e)^2} = \frac{A'}{e^2} \tag{B5}$$

and therefore,

$$\phi' = \frac{LA'A_D}{e^2} \tag{B6}$$

where L is still undetermined.

Except for the directly irradiated area A_I, the inside sphere wall is uniformly illuminated by an irradiance $E/(W/m^2)$ given by the following argument.

Let r equal the diffuse reflectance of the sphere walls. Then, the flux distributed inside the sphere after the initial reflection from A_I is

$$\phi_1 = r\phi \tag{B7}$$

Of this, the fraction $(A+A')/A_s$ is lost through the holes. Hence, the flux due to the second reflection is

$$\phi_2 = r[1 - (A+A')/A_s] \phi_1 \tag{B8}$$
$$= r^2[1 - (A+A')/A_s] \phi \tag{B9}$$

21

Again, a fraction $(A+A')/A_S$ is lost so that

$$\phi_3 = r[1 - (A+A')/A_S] \, \phi_2 \qquad , \qquad \text{(B10)}$$

$$= r^3[1 - (A+A')/A_S]^2 \, \phi \qquad . \qquad \text{(B11)}$$

Generally,

$$\phi_n = r^n[1 - (A+A')/A_S]^{n-1} \, \phi \qquad \text{(B12)}$$

Therefore, the irradiance of the sphere wall is

$$E = \frac{\phi_1 + \phi_2 + \cdots}{A_S} \qquad \text{(B13)}$$

$$= (r\phi/A_S) \left\{ 1 + r[1-(A+A')/A_S] + r^2[1-(A+A')/A_S]^2 + \cdots \right\} \qquad \text{(B14)}$$

$$E = \frac{r\phi/A_S}{1 - r[1 - (A+A')/A_S]} \qquad \text{(B15)}$$

This irradiance causes a diffuse radiance

$$L = rE/\pi \qquad \text{(B16)}$$

of the inside sphere walls. Combining equations B6, B15, and B16, we obtain the desired efficiency of the averaging sphere.

$$\epsilon = \frac{(A'A_D)/\pi e^2 \, A_S r^2}{1 - r[1 - (A+A')/A_S]} \qquad \text{(B17)}$$

which was used as Eq. 3, above.

References

[1] Reader, J., J. Res. Nat. Bur. Stand. (U.S.), 53, 243 (1969).

[2] These measurements were made by Mr. J. C. Schleter of NBS.

[3] This experiment was done with the aid of Dr. J. Reader of NBS.

[4] Mielenz, K.D., J. Res. Nat. Bur. Stand. (U.S.), to be published.

[5] Mielenz, K.D., Eckerle, K.L., Reader, J., and Madden, R. P. (to be published).

[6] The light beam in our monochromator travels in the reverse direction, i.e., the entrance aperture became our exit aperture and vice versa. This was done so that the monochromator controls would be accessible from the source side. The predisperser drive (which is coupled to the monochromator) was modified accordingly so that the monochromator screw and predisperser would be linked together.

[7] Saunders, J.B., J. Res. Nat. Bur. Stand. (U.S.), 68C, 155 (1964).

[8] Taylor, D.J., Rev. Sci. Instr., 40, 559 (1969).

[9] Certain commercial instruments or materials are identified in this paper in order to specify adequately the procedure. In no case does such identification imply endorsement or evaluation by the National Bureau of Standards.

[10] Estimating Stray Radiant Energy, 1970 Annual Book of ASTM Standards, Part 30, p. 1154 (1970).

[11] Mielenz, K.D., and Eckerle, K.L., (scheduled to be published in Appl. Optics in October, 1972).

[12] Photomultiplier Manual (RCA Electronic Components, Harrison, N.J., 07029, 1970), p. 65.

[13] The manufacturer quotes the "typical" gain of the dynode chain as $\delta^{11} = 2 \times 10^6$, hence, $\delta = 3.7$. He also states that, for CsSb dynodes, δ has the empirical form $\delta = 0.2 \ V^{0.7}$, where V is the interdynode voltage. Hence, for a total applied voltage of 850 V, $V = 850/12 = 70$ V and $\delta = 3.9$.

[14] This analysis was done with the aid of Mr. J. M. Cameron, of NBS.

[15] Menis, O., and Schultz, J.I., (Editors), Nat. Bur. Stand. (U.S.), Tech. Note 584 (1971).

Table I

Item	Model Number	Manufacturer
Lamp	18A/T10/1 SR8	General Electric
Lamp Power Supply	KS18-50(M)	Kepco
Neutral wedge	A6020	Eastman Kodak
Predisperser	Model 608	McPherson
Monochromator	Model 2051	McPherson
Parabolic mirrors	Special	Ferson
High Voltage Power Supply	412B	Fluke
Counter	1192/z	General Radio
Data Acquisition and Control System	Special	Compumetrics
Photomultiplier	9558QA	EMI
Shunt (0.1Ω, 50A)	4360	Leed and Northrup

Table II

Final Values of σ and ΔT Obtained by Repeated
Measurements ($\lambda = 525$ nm, $I(\phi) = 3 \times 10^{-7}$ A)

T	First Measurement		Second Measurement	
	$\sigma \times 10^4$	$\Delta T \times 10^4$	$\sigma \times 10^4$	$\Delta T \times 10^4$
0.1	0.07	0.72	0.19	0.77
0.2	0.25	1.38	0.45	1.46
0.3	0.52	1.96	0.79	2.02
0.4	0.91	2.40	1.21	2.43
0.5	1.39	2.67	1.70	2.66
0.6	1.97	2.73	2.27	2.68
0.7	2.66	2.53	2.92	2.45
0.8	3.45	2.04	3.65	1.95
0.9	4.34	1.21	4.45	1.14
1.0	5.34	0.00	5.33	0.00

Table III

Measured Non-Linearity Correction ΔT
for Different Operating Conditions
for Spectrophotometer $(I(\phi)=3\times10^{-7}A)$

$\Delta T \times 10^4$

T	525 nm 0°	525 nm 90°	525 nm ±45°	400 nm	750 nm
0.1	0.75	0.73	0.75	0.80	0.59
0.2	1.42	1.41	1.40	1.53	1.17
0.3	1.98	1.99	1.92	2.15	1.70
0.4	2.37	2.45	2.28	2.62	2.14
0.5	2.67	2.72	2.48	2.90	2.43
0.6	2.70	2.78	2.47	2.94	2.52
0.7	2.49	2.58	2.25	2.74	2.37
0.8	1.99	2.08	1.78	2.18	1.94
0.9	1.18	1.23	1.04	1.28	1.12

Table IV

Transmittance of Nominal 10% Filter

	440 nm	465 nm	590 nm	635 nm
R. Mavrodineanu (Lab 1)	.1159	.1356	.1037	.1136
Mielenz and Eckerle (Lab 2)				
Alignment 1 - Run 1	.11448	.13391	.10244	.11217
Alignment 2 - Run 2	.11516	.13467	.10297	.11275
Alignment 2 - Run 3	.11511	.13462	.10295	.11278
(Lab 1) - (Lab 2)				
Run 1	.00142	.00169	.00126	.00143
Run 2	.00074	.00093	.00073	.00085
Run 3	.00079	.00098	.00075	.00082
Change in transmittance between parallel and perpendicular polarization				
Run 1	-.00008	-.00001	.00000	+.00003
Run 2	-.00005	+.00001	-.00001	+.00001
Run 3	-.00005	+.00010	-.00014	-.00016

Table V

Transmittance of Nominal 20% Filter

	440 nm	465 nm	590 nm	635 nm
R. Mavrodineanu (Lab 1)	.1980	.2259	.1916	.2060
Mielenz and Eckerle (Lab 2)				
Alignment 1 - Run 1	.19795	.22587	.19161	.20608
Alignment 2 - Run 2	.19811	.22602	.19170	.20618
Alignment 2 - Run 3	.19805	.22595	.19168	.20617
(Lab 1) - (Lab 2)				
Run 1	+.00005	+.00003	-.00001	-.00008
Run 2	-.00011	-.00012	-.00010	-.00018
Run 3	-.00005	-.00005	-.00008	-.00017
Change in transmittance between parallel and perpendicular polarization				
Run 1	+.00001	-.00003	+.00001	+.00007
Run 2	-.00009	-.00004	-.00003	+.00006
Run 3	+.00018	+.00017	+.00006	+.00004

Table VI

Transmittance of Nominal 30% Filter

	440 nm	465 nm	590 nm	635 nm
R. Mavrodineanu (Lab 1)	.3287	.3553	.3113	.3255
Mielenz and Eckerle (Lab 2)				
Alignment 1 - Run 1	.32893	.35566	.31154	.32581
Alignment 2 - Run 2	.32901	.35577	.31154	.32593
Alignment 2 - Run 3	.32902	.35566	.31153	.32592
(Lab 1) - (Lab 2)				
Run 1	-.00023	-.00036	-.00024	-.00031
Run 2	-.00031	-.00047	-.00024	-.00043
Run 3	-.00032	-.00036	-.00023	-.00042
Change in transmittance between parallel and perpendicular polarization				
Run 1	-.00001	+.00003	+.00009	-.00004
Run 2	-.00022	+.00001	-.00003	+.00006
Run 3	-.00002	.00000	-.00008	-.00003

Table VII

Range of Transmittance of Filters When
Area Measured is Varied at 635 nm with a
2 mm by 12 mm Aperture and Parallel Polarization

	−1 mm	0 mm (Central Position)	+1 mm
Nominal 10% Filter	.11247	.11270	.11301
Nominal 20% Filter	.20601	.20619	.20641
Nominal 30% Filter	.32593	.32591	.32600

Range for 10% Filter = 0.00054

Range for 20% Filter = 0.00040

Range for 30% Filter = 0.00009
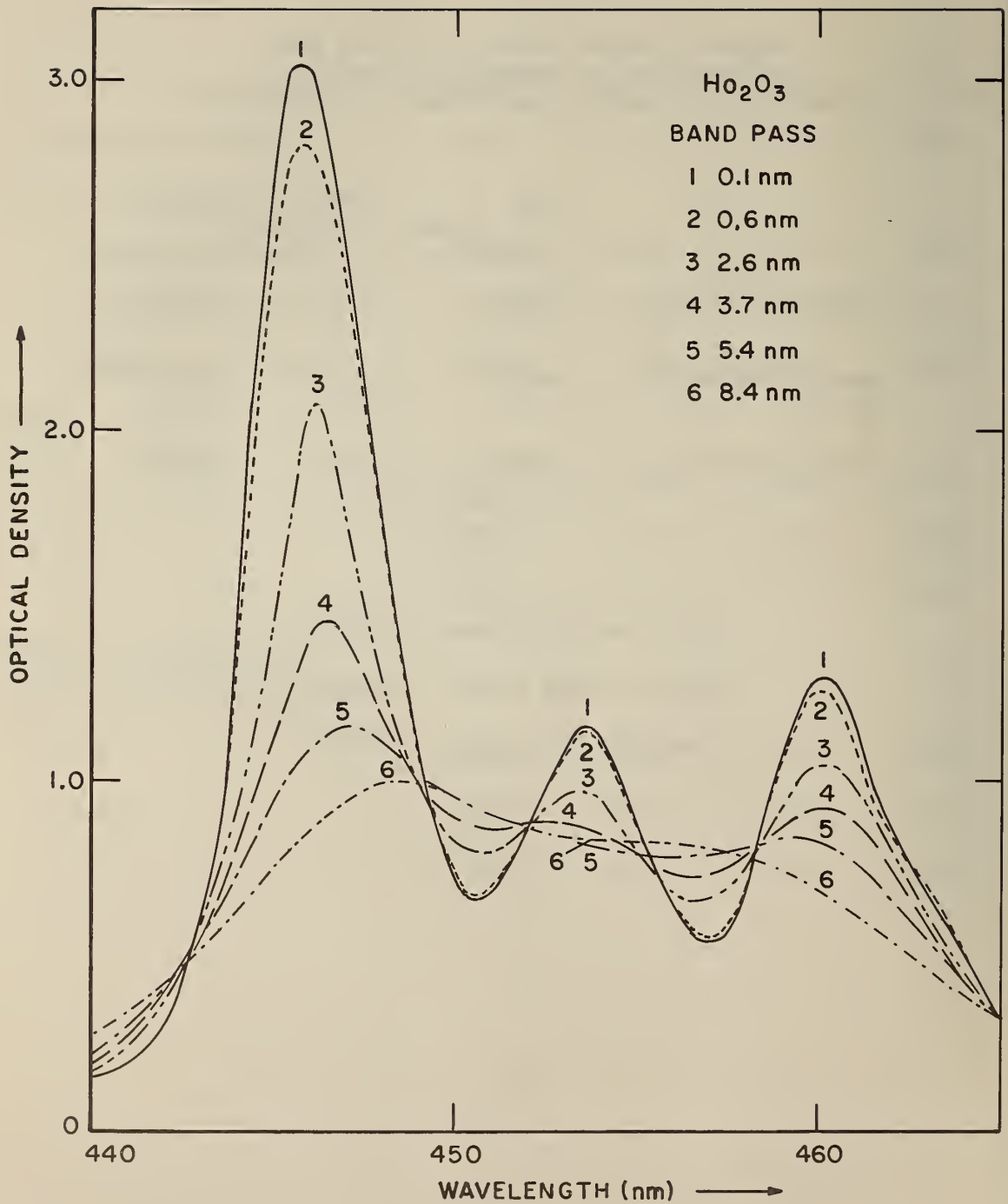
Fig. 1. Measured spectra of a holmium oxide glass filter.
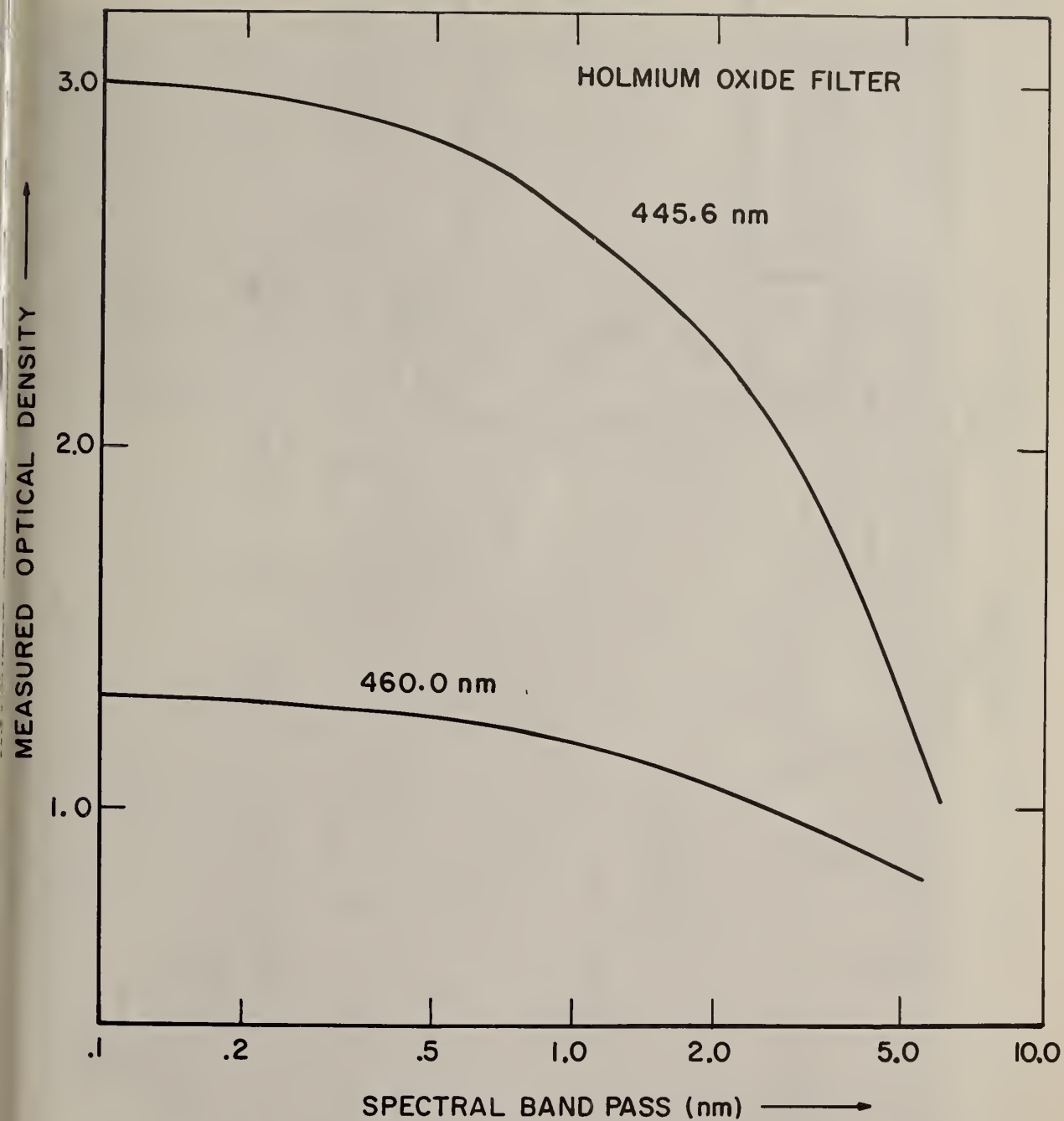
Fig. 2. Variation of measured optical density with spectral bandpass of the holmium oxide glass filter.
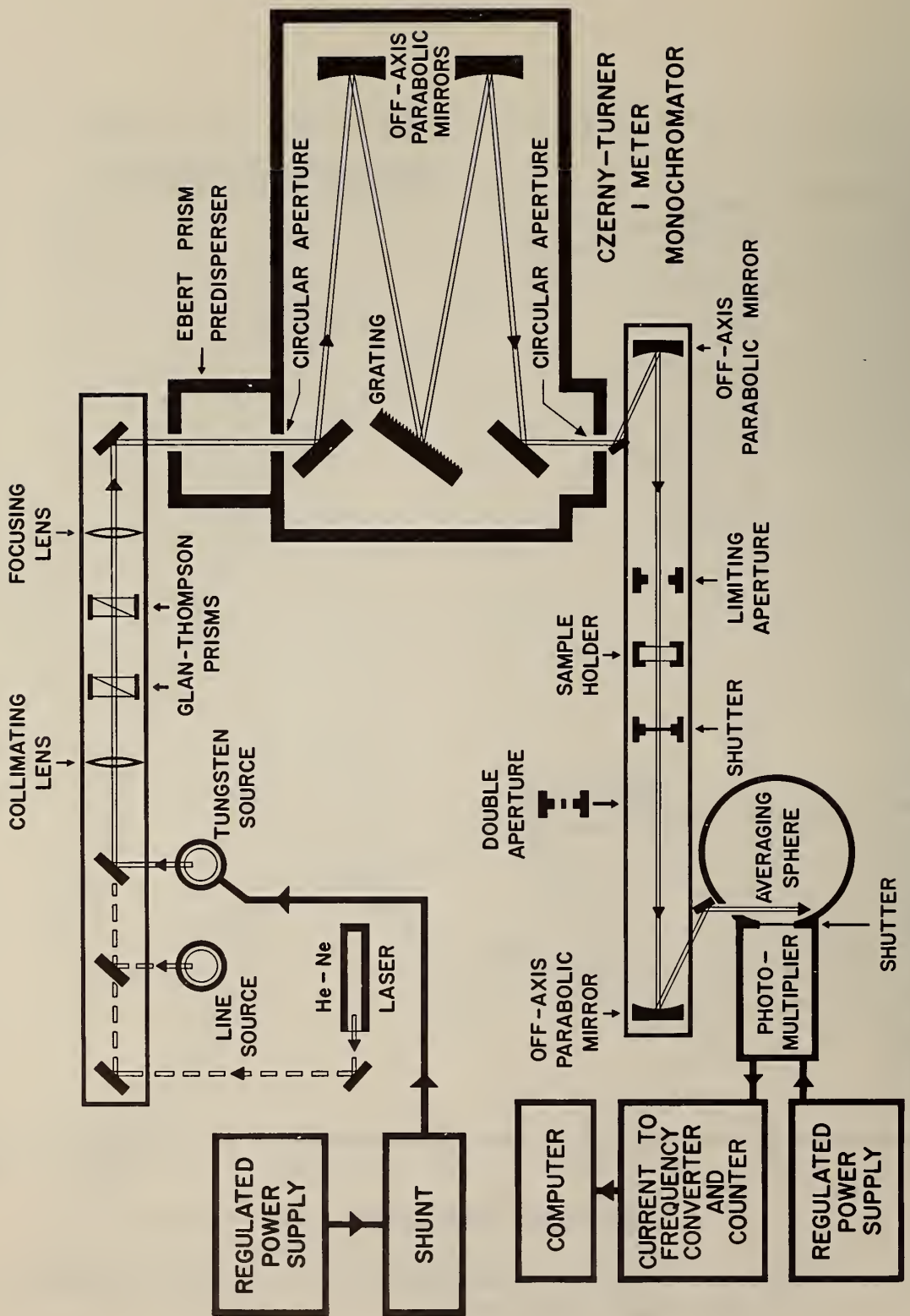
Fig. 3. Schematic Diagram of Spectrophotometer.

34
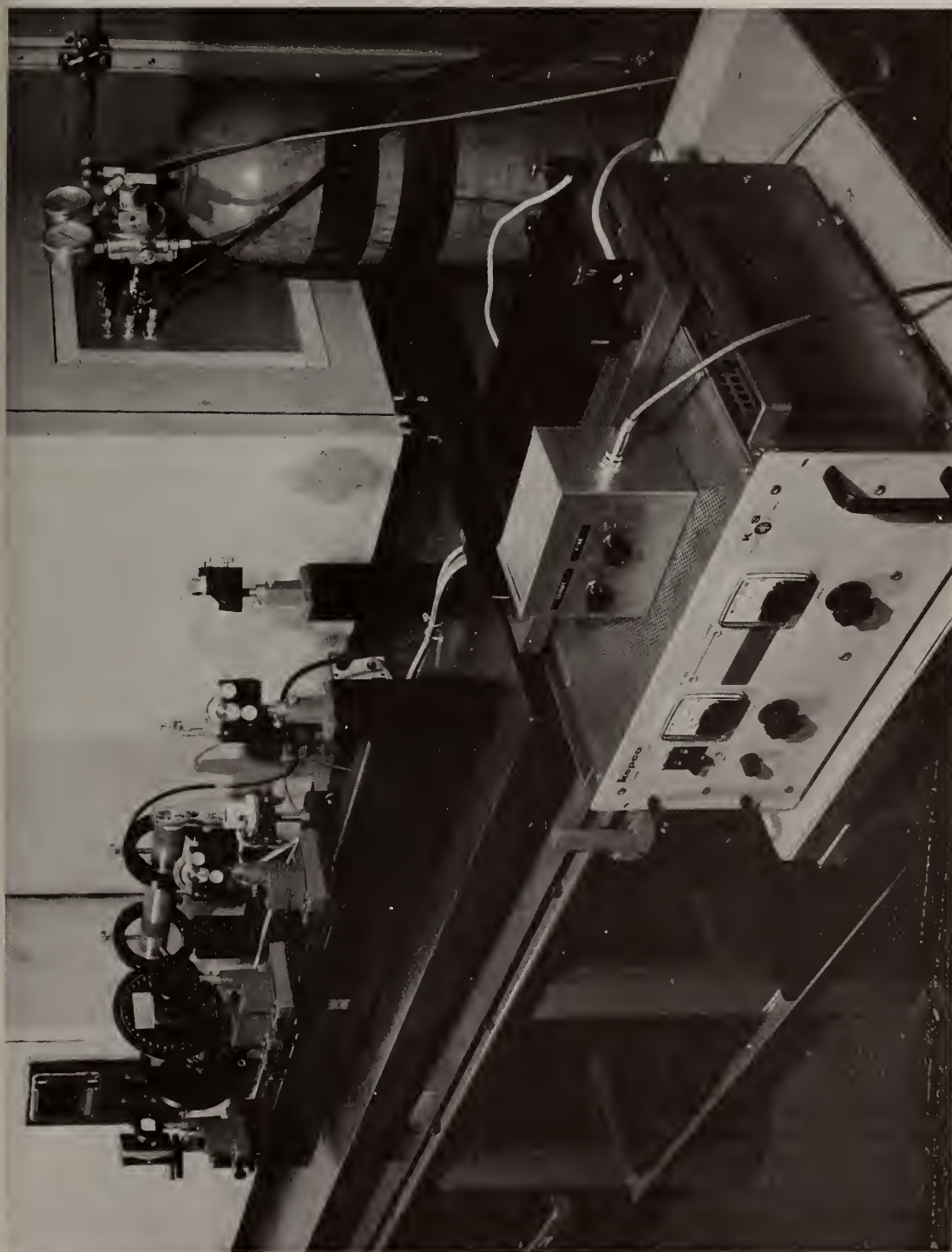
Fig. 4. Source Arrangement of Spectrophotometer.

35
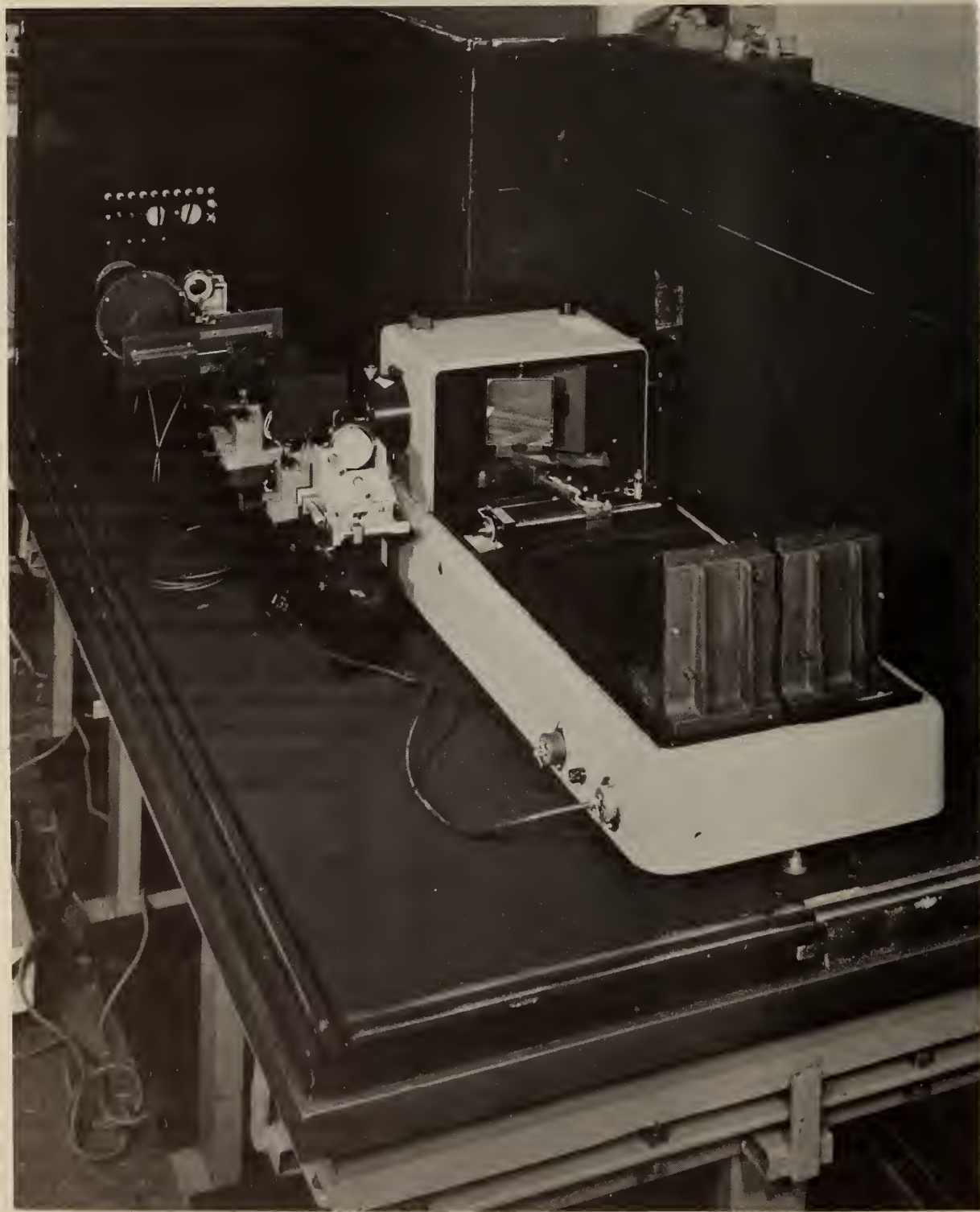
Fig. 5. Exit Arrangement and Detector of Spectrophotometer.

Fig. 6. Control Panel and Electronics.

37
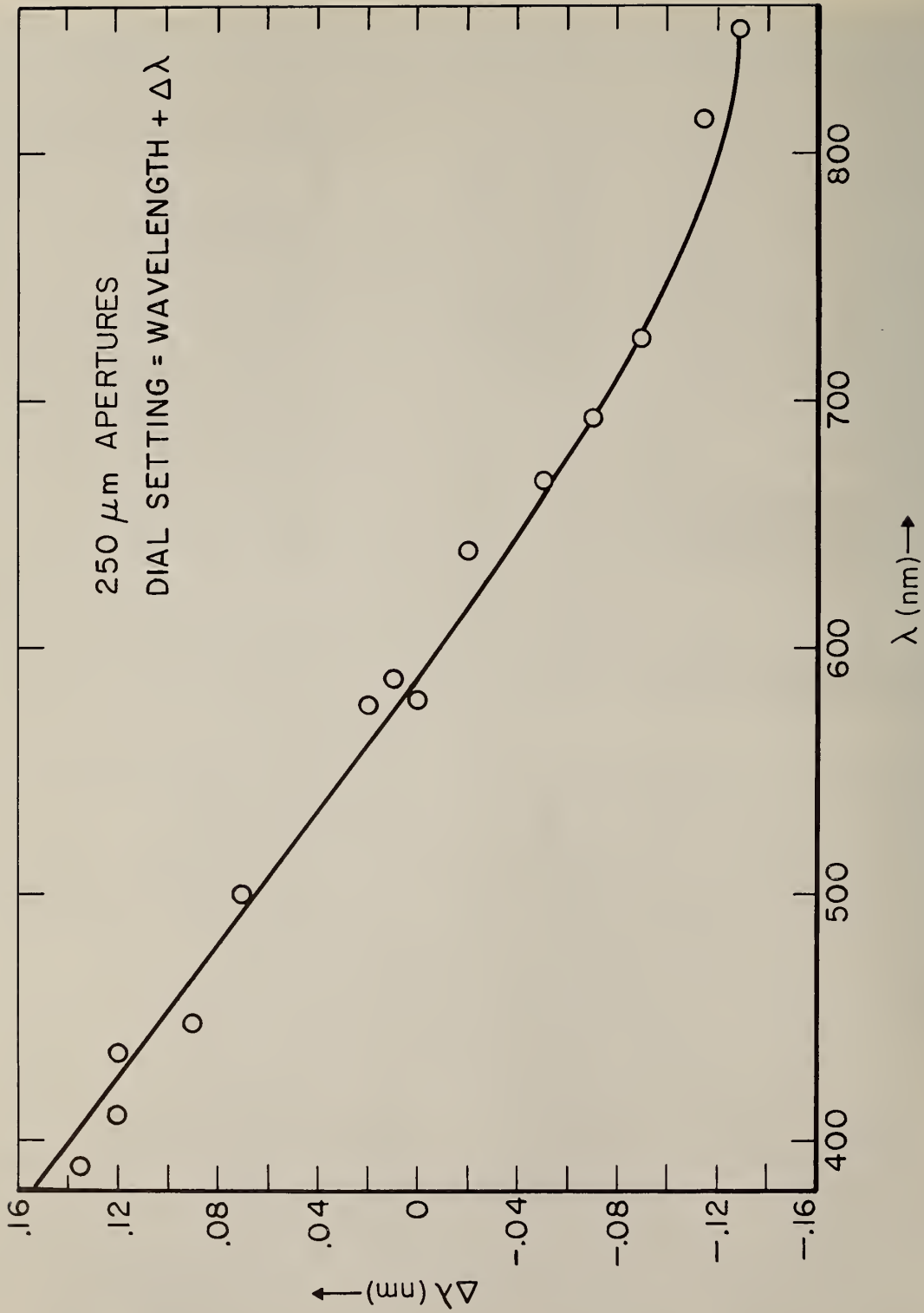
Fig. 7. Wavelength Calibration Curve for 250 μm Apertures.

38
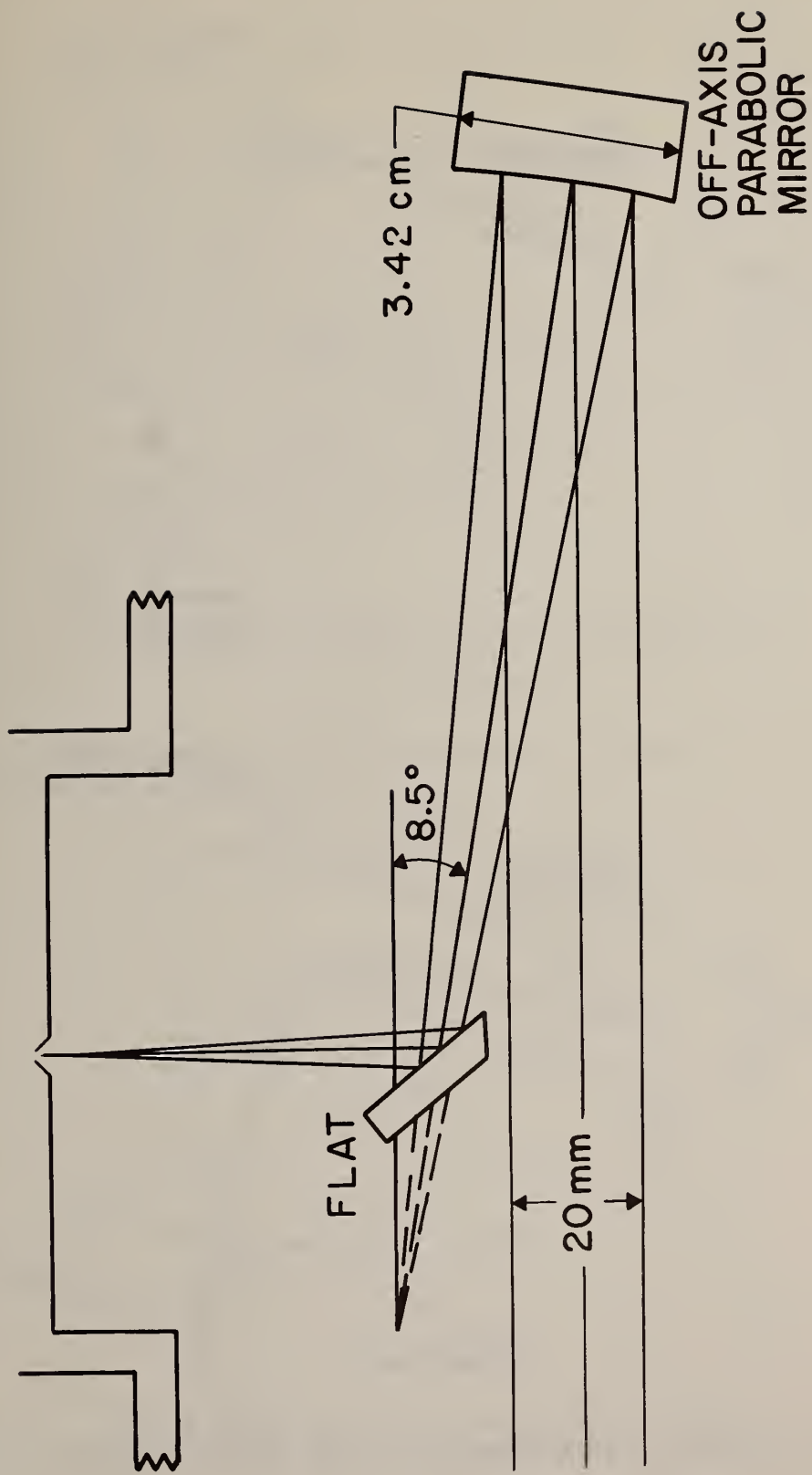
Fig. 8. Optical Path of Light Leaving Monochromator.
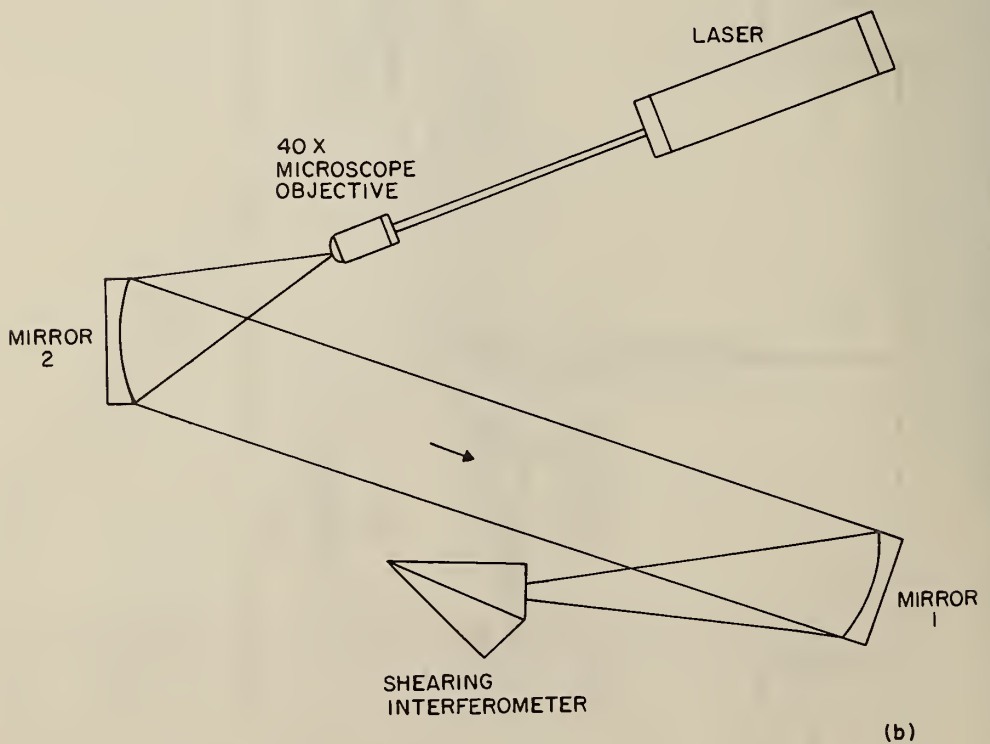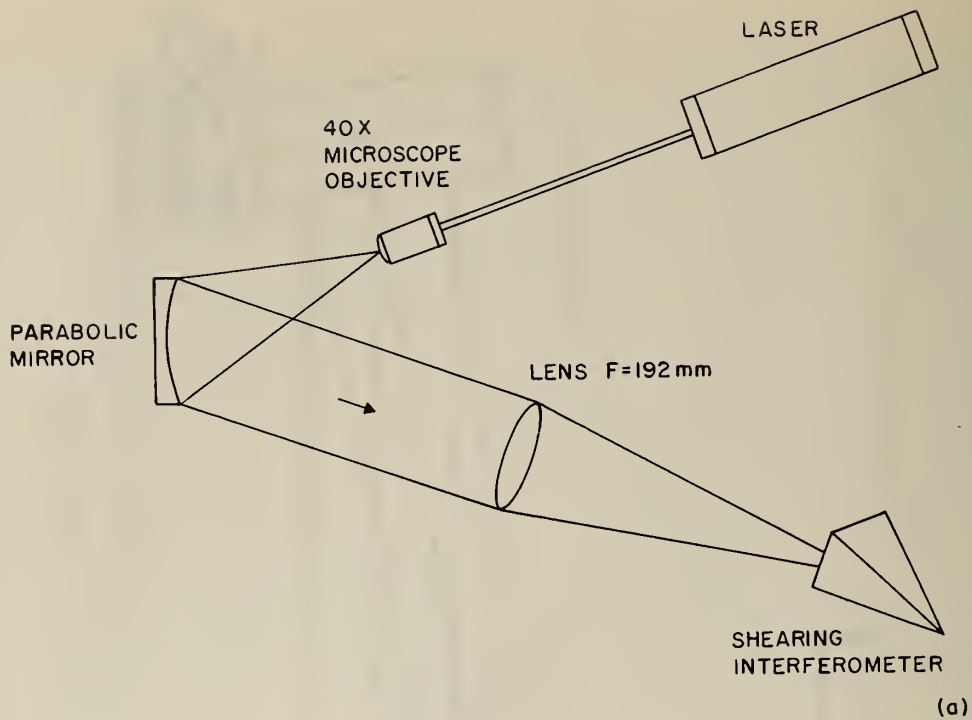
Fig. 9. Use of Shearing Interferometer to Check Off-axis Parabolic Mirrors.

(a) Individually
(b) Both mirrors in "z" arrangement

40
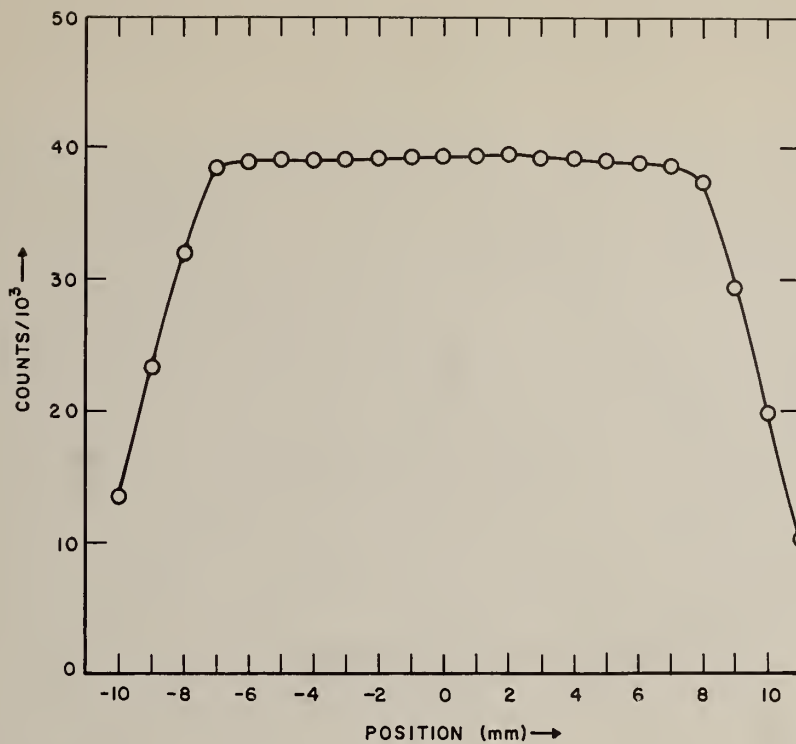
Fig. 10. Nonuniformity of spectrophotometer light beam; scan parallel to grating grooves at 632.8 nm.
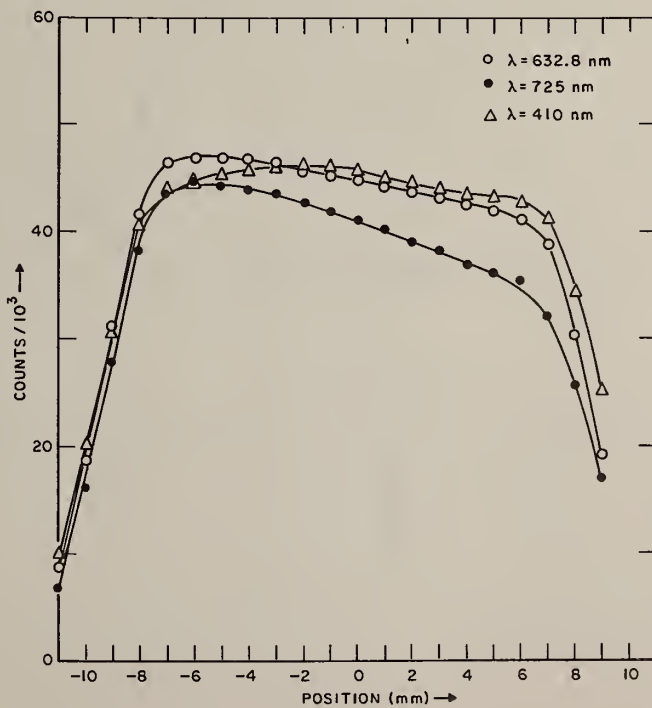
Fig. 11. Nonuniformity of spectrophotometer light beam; scan perpendicular to grating grooves at 410 nm, 632.8 nm, and 725 nm.
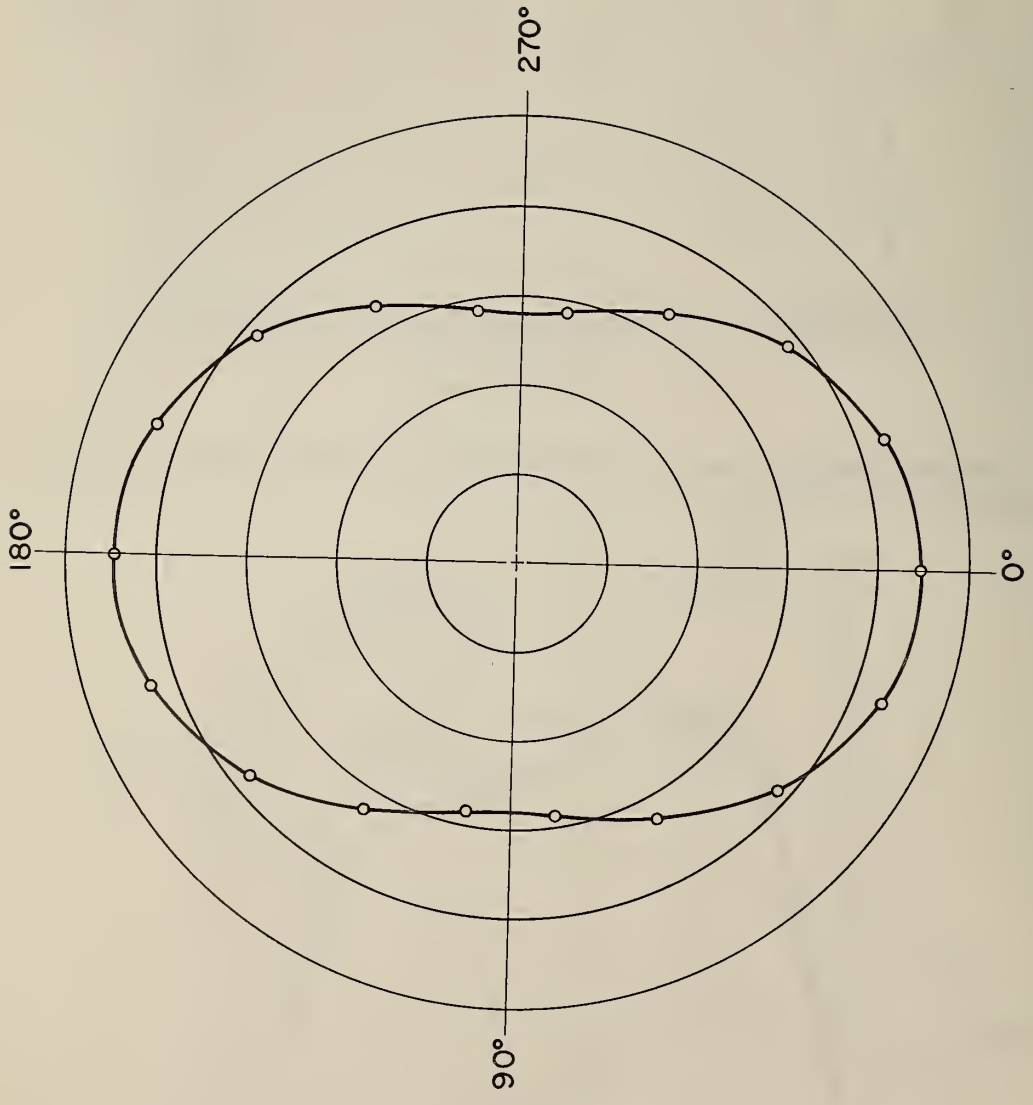
Fig. 12. Partial polarization of spectrophotometer light beam at 564 nm. Transmittance of sheet polarizer is plotted on arbitrary scale.

42
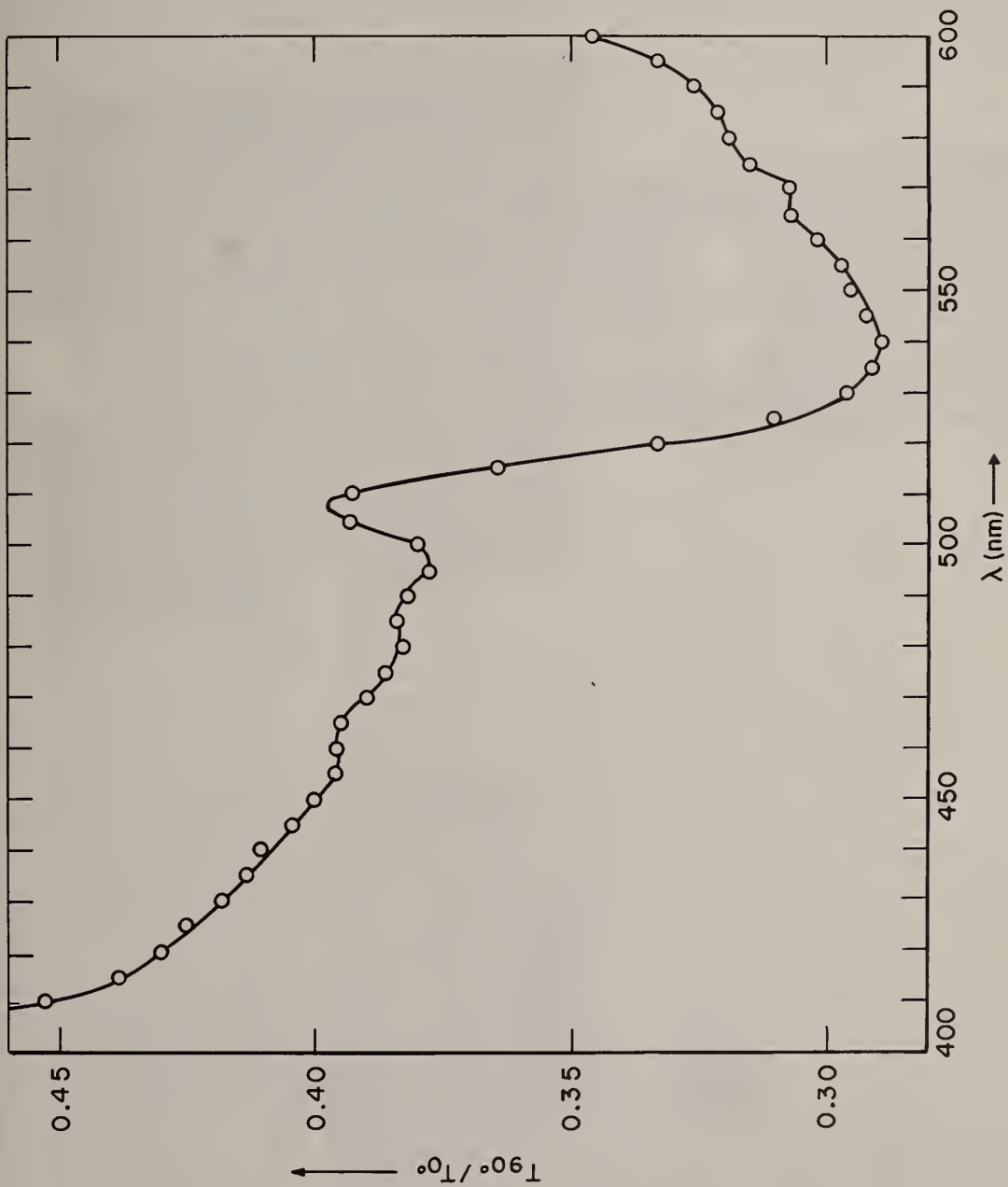
Fig. 13. Polarization of Predisperser and Monochromator with Xenon Arc Source.

Axis labels: λ (nm) →, $T_{90°}/T_{0°}$ →

43

Fig. 14.   Double Aperture Linearity Device.

44

BaSO₄

ILLUMINATED
AREA
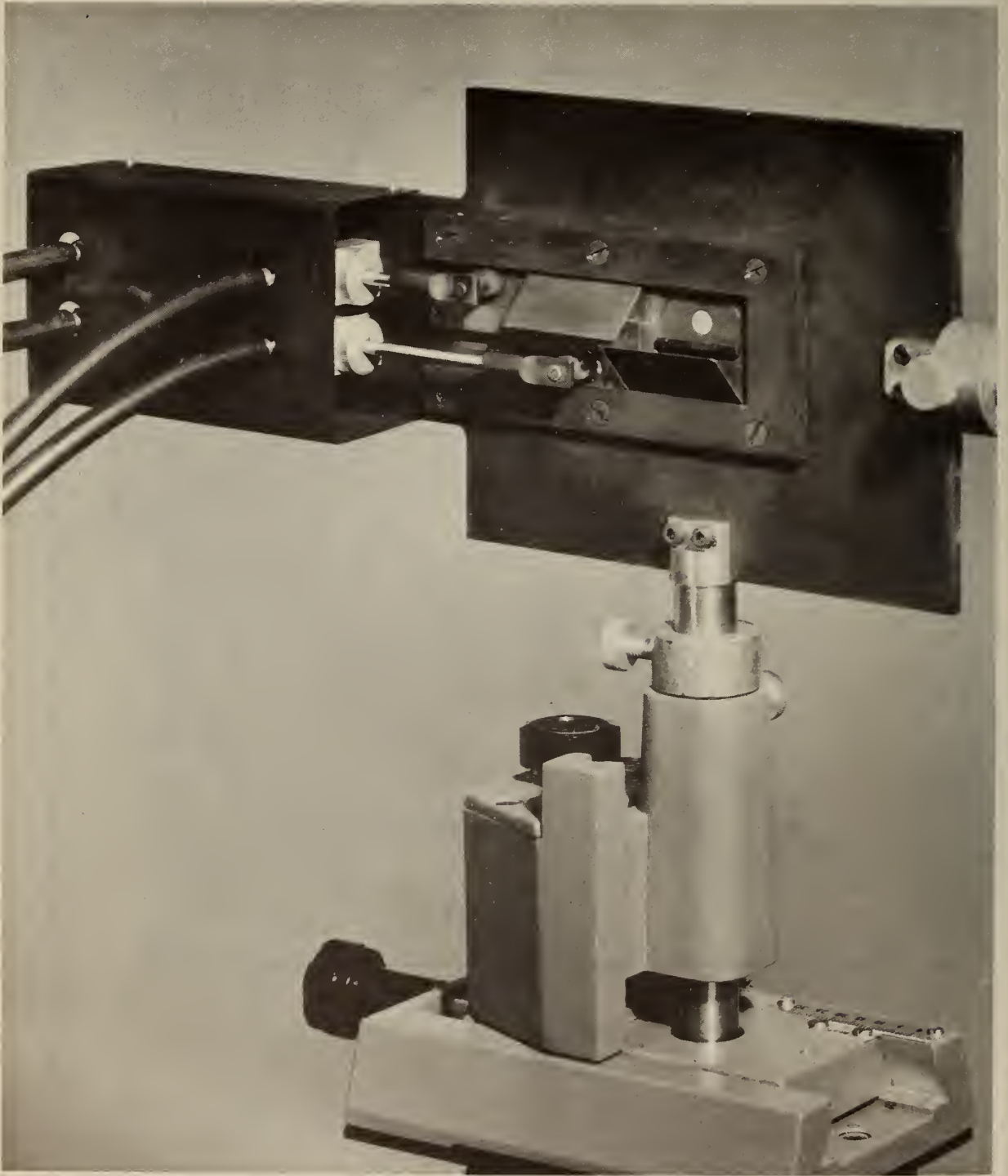
PHOTOMULTIPLIER
CATHODE
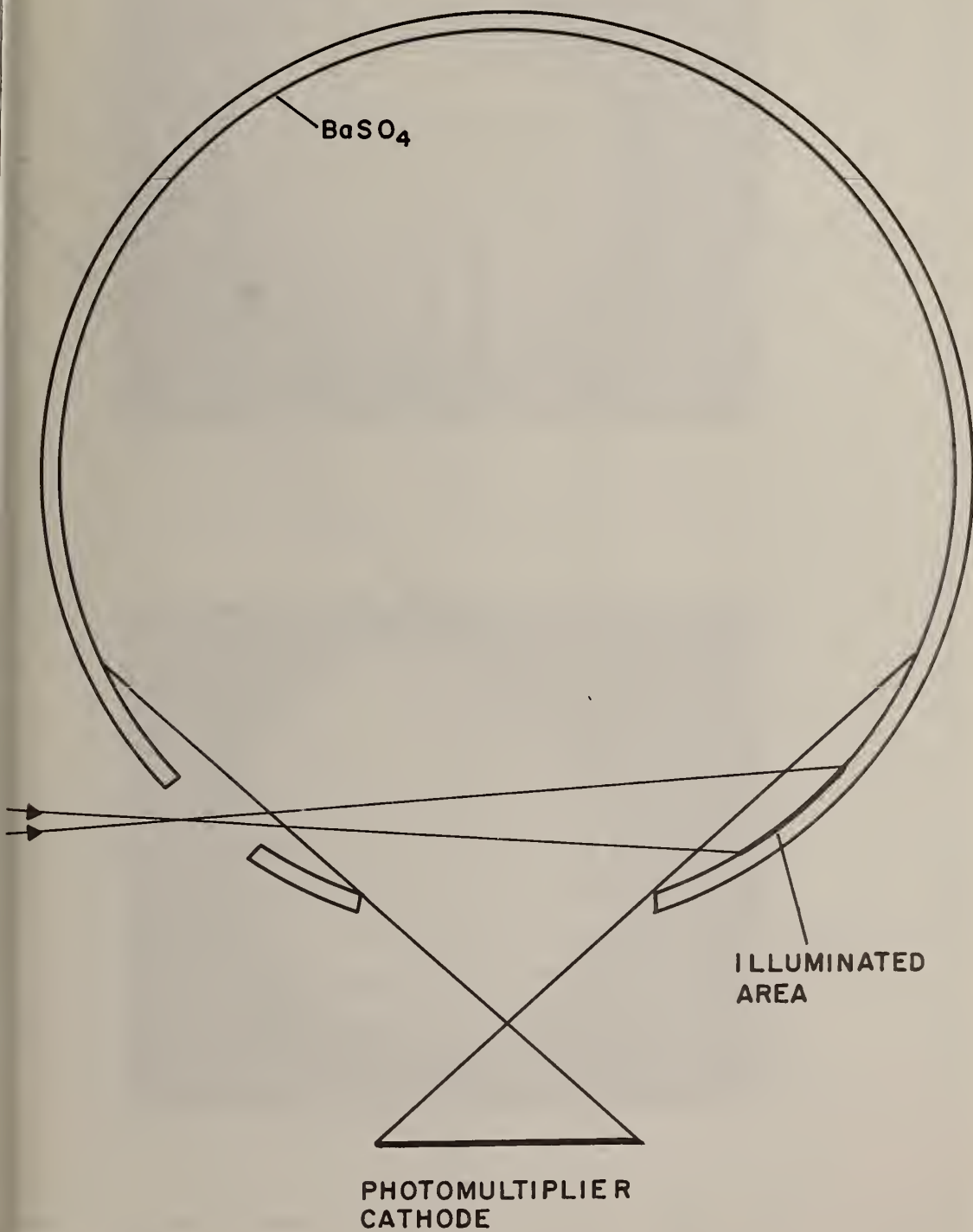
Fig. 15. Geometry of Averaging Sphere and Incident Light.

45
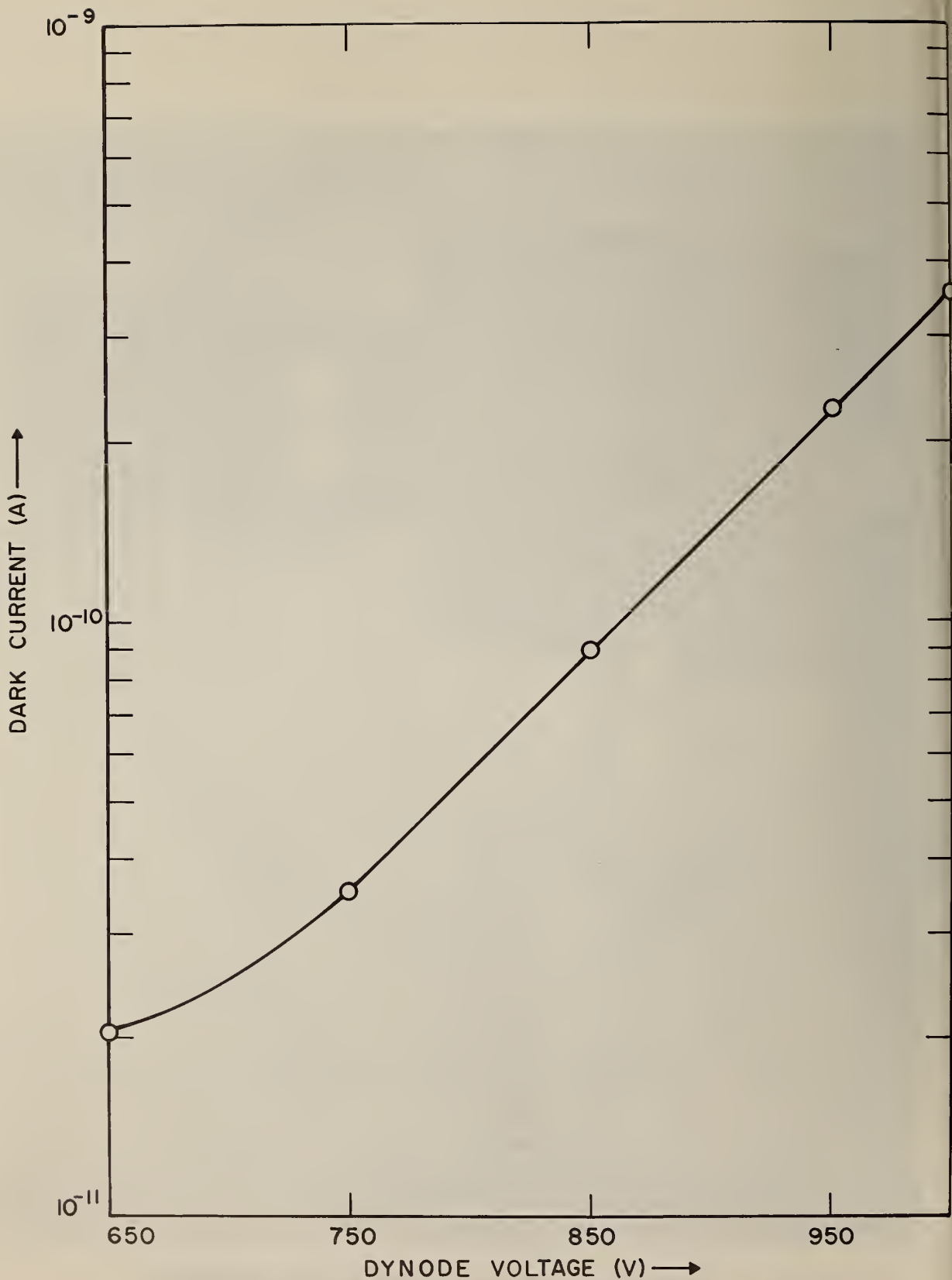
Fig. 16.   Dark Current of Photomultiplier Tube.

46

GROOVES

a

GROOVES

b

Fig. 17. Twyman-Green Interferometer Photographs of Grating.
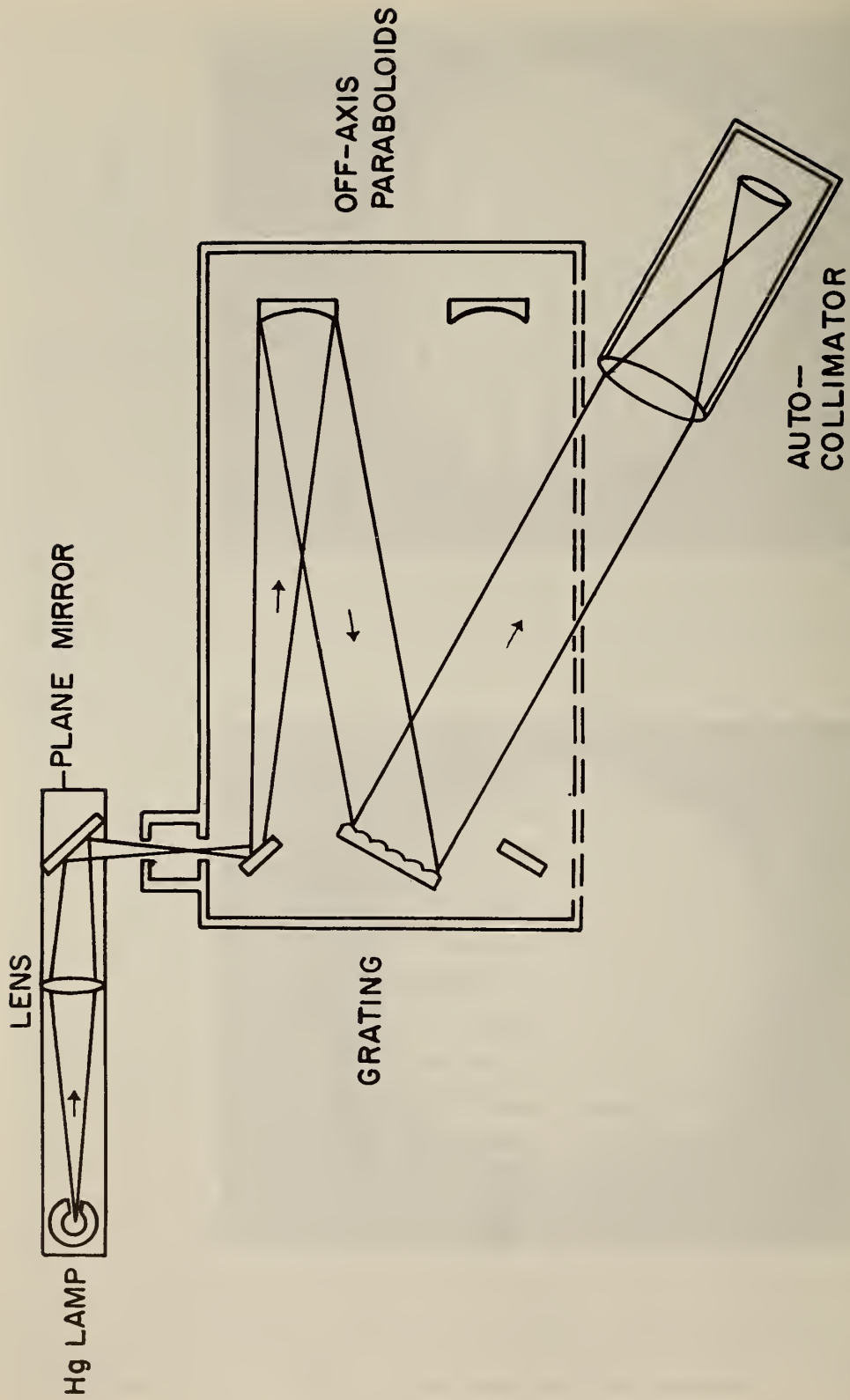
(a) Parallel to the grooves
(b) Perpendicular to the grooves

47

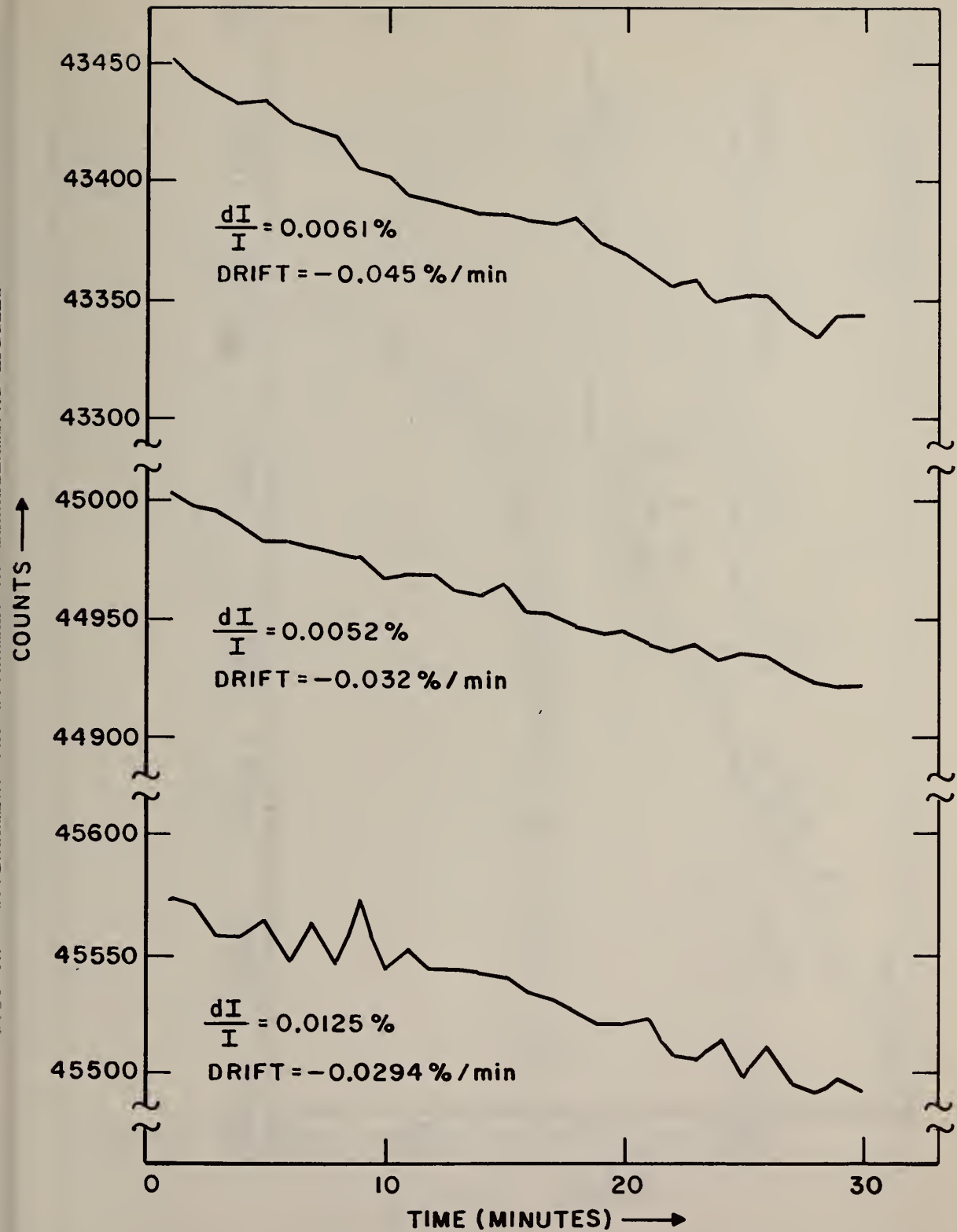Fig. 18. Arrangement for Alignment of Monochromator Mirrors.
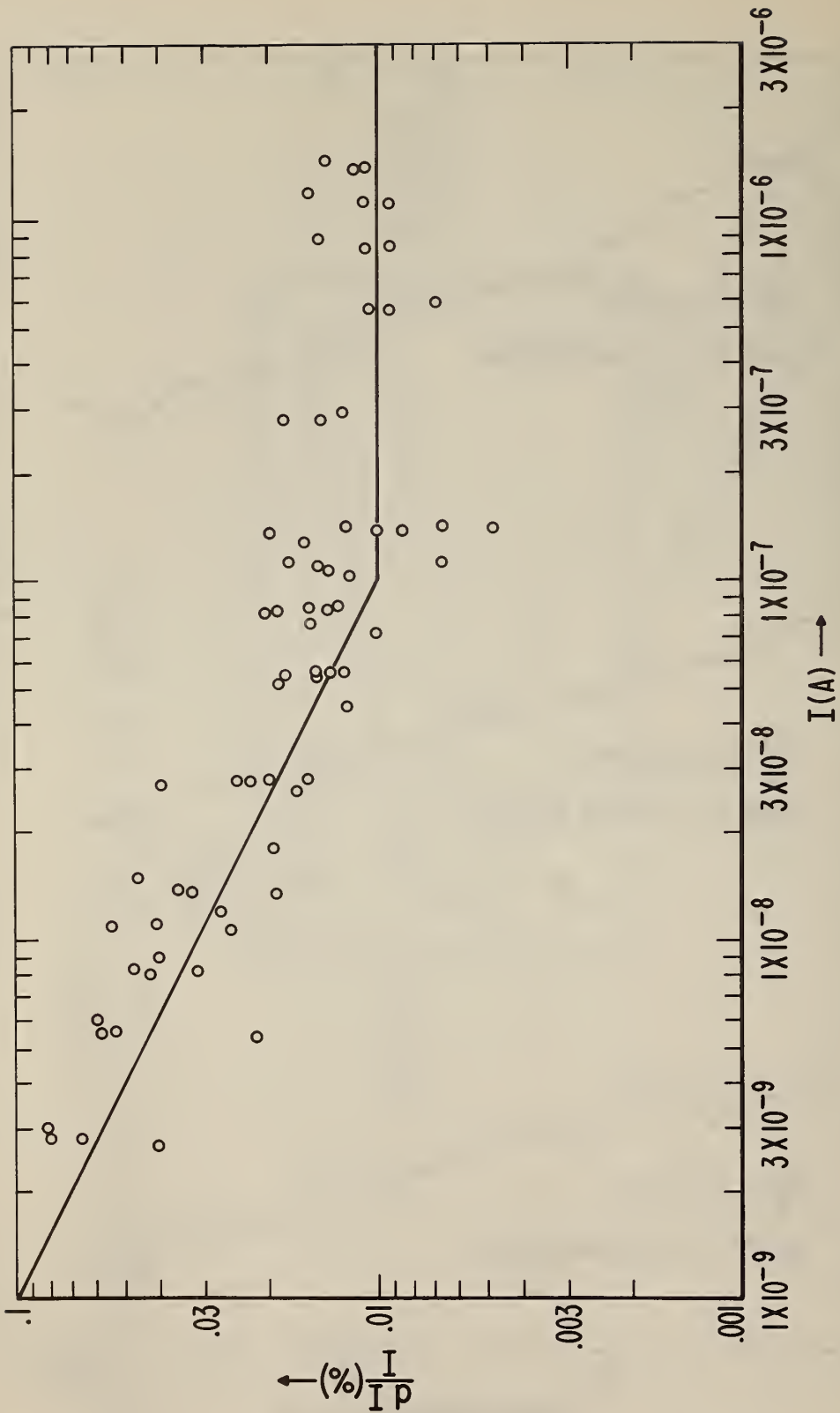
48

Fig. 19. System Drift as a Function of Time.

49

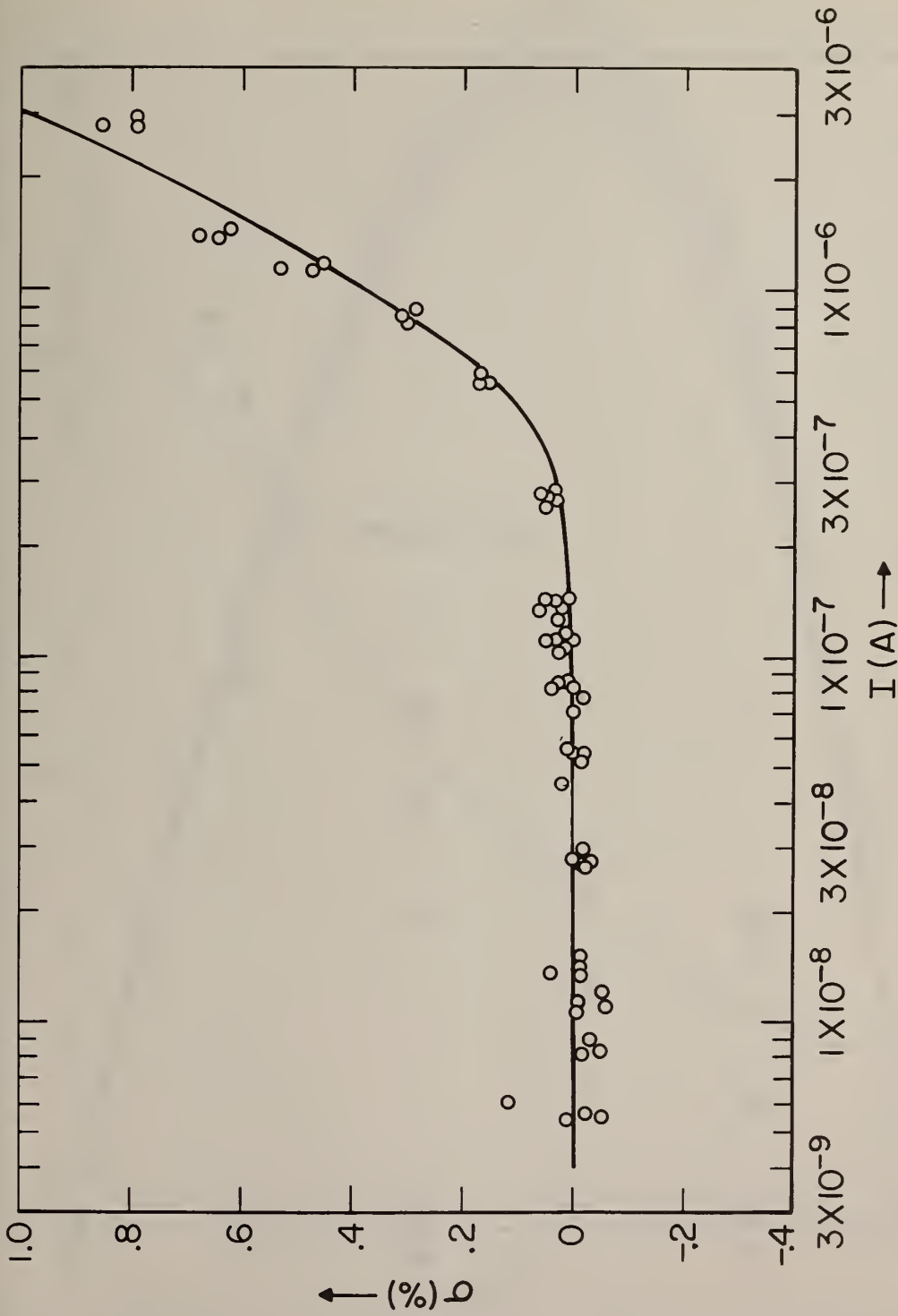Fig. 20. Logarithmic plot of photometric precision dI/I of spectrophotometer versus signal current I.

Fig. 21. Semi-logarithmic plot of nonlinearity term σ for $A = B = \frac{1}{2} \phi$ versus signal current $I(\phi)$.
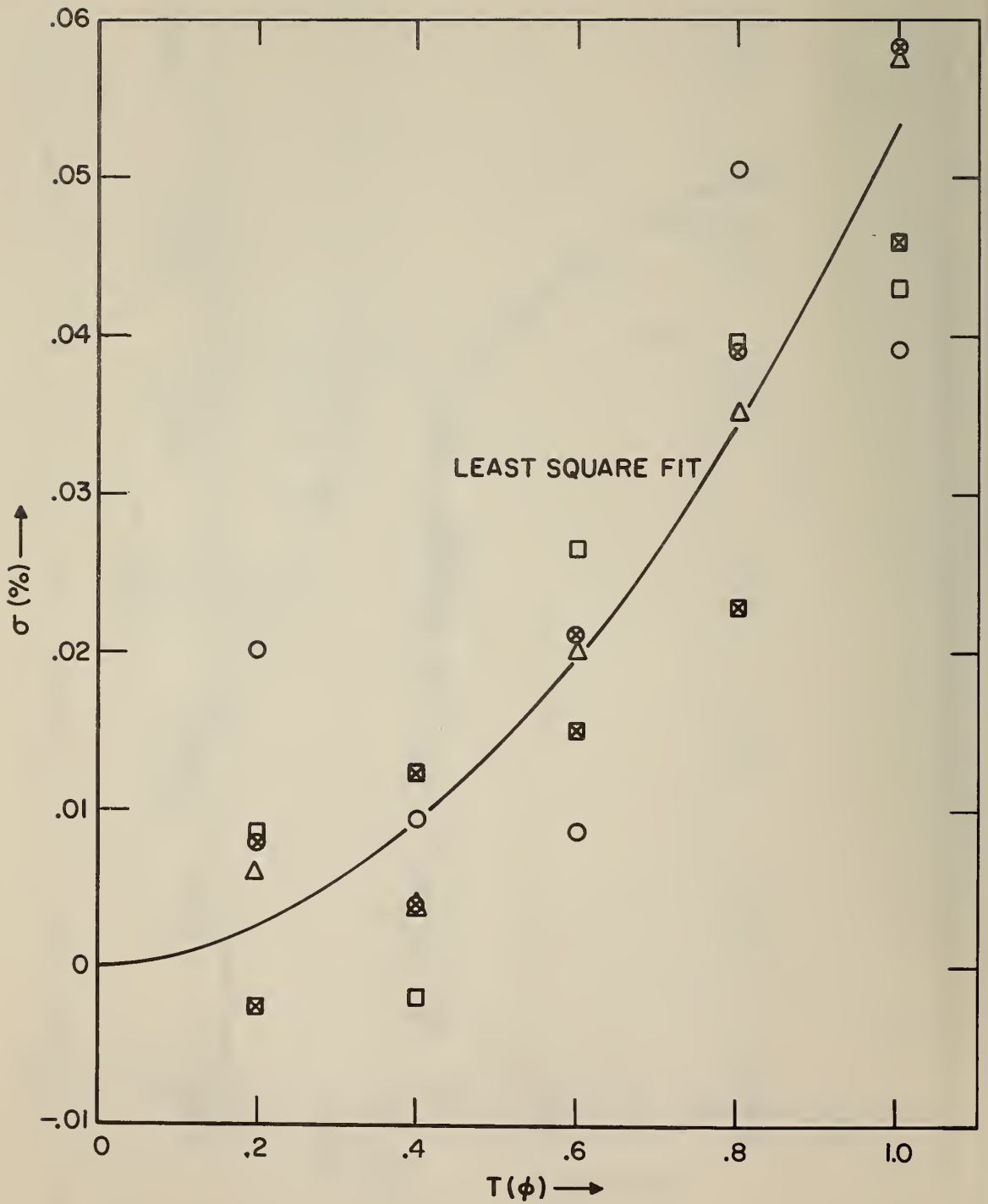
Fig. 22. Measured dependence of $\sigma(T\phi)$ on T for $I(\phi) = 3 \times 10^{-7}$ A and $\lambda = 525$ nm.

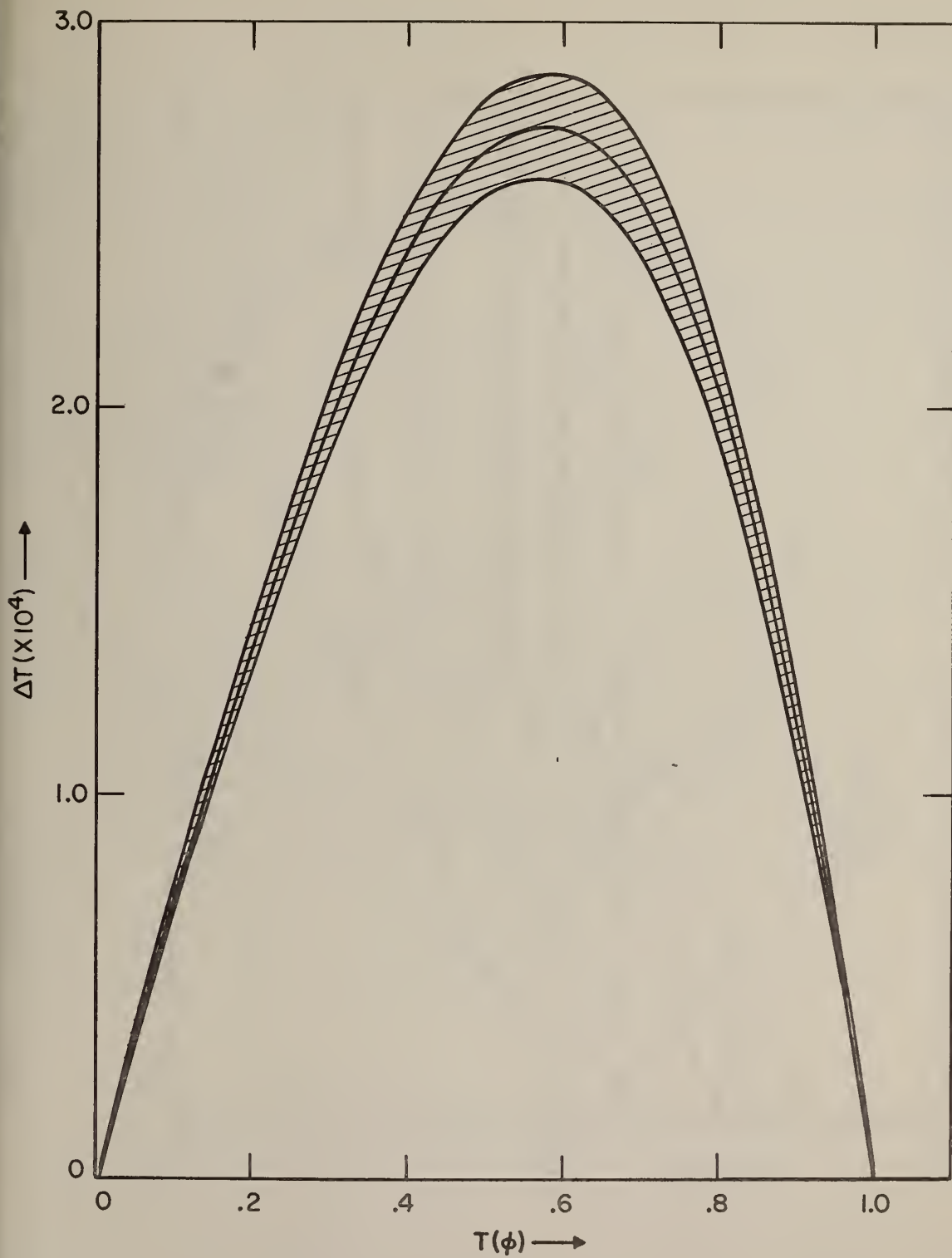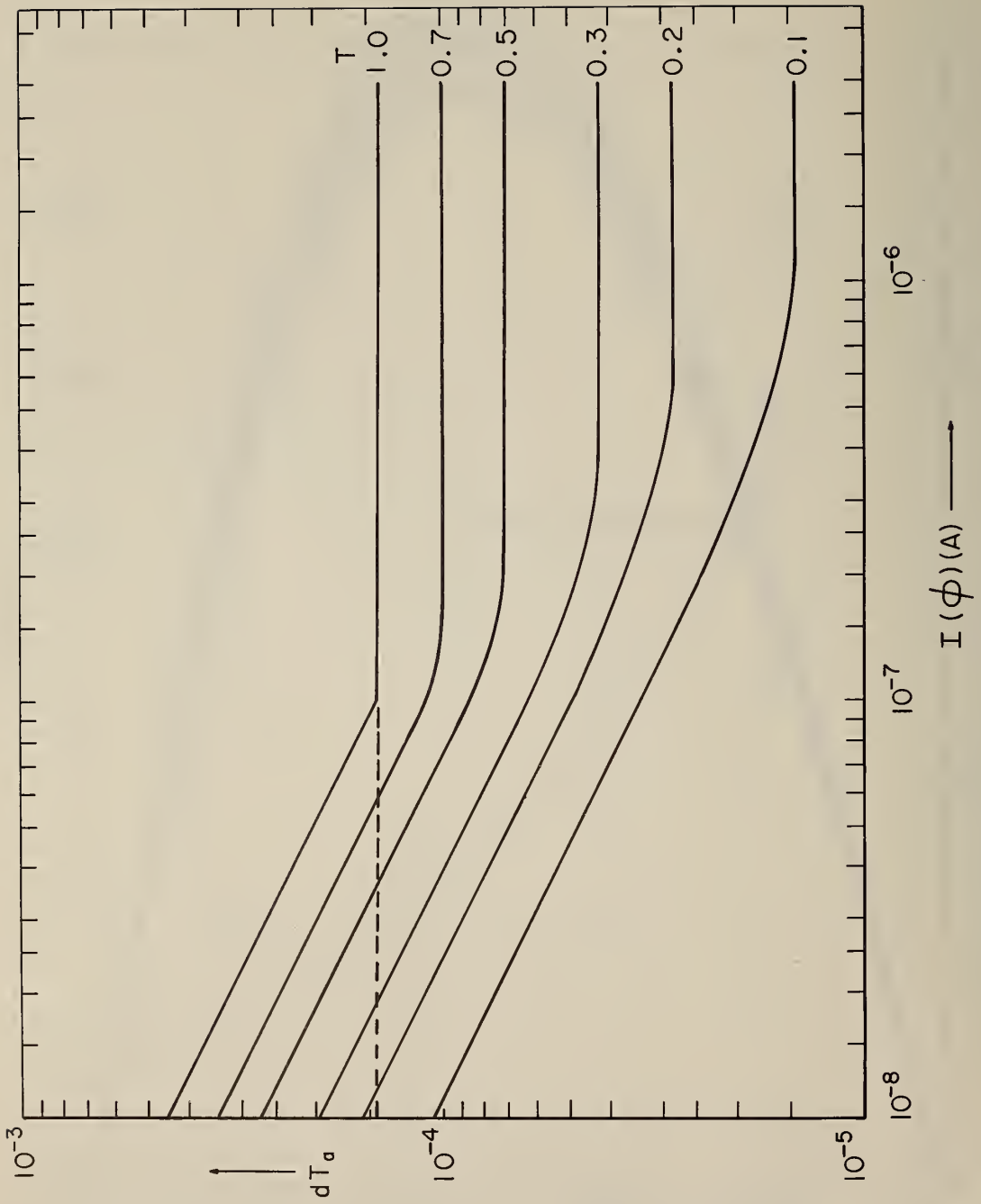Fig. 23. Nonlinearity correction ΔT computed from measured data in Fig. 22.

53

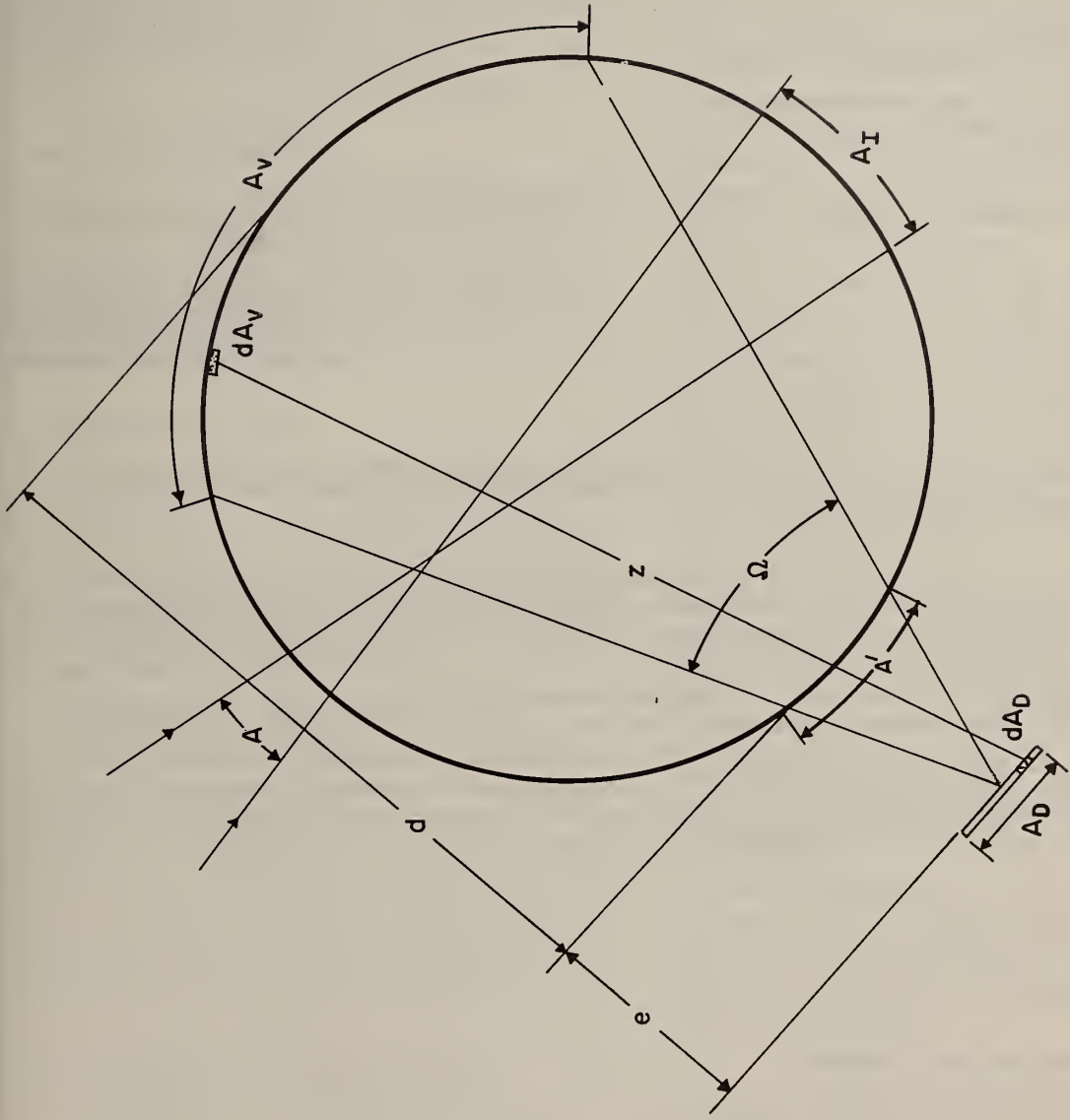Fig. 24. Random errors in transmittance dT_a versus anode current $I(\phi)$.

54

Fig. 25. Parameters for calculating efficiency of averaging sphere.

U.S. DEPT. OF COMM. BIBLIOGRAPHIC DATA SHEET	1. PUBLICATION OR REPORT NO. NBS TN-729	2. Gov't Accession No.	3. Recipient's Accession No.
4. TITLE AND SUBTITLE DESIGN, CONSTRUCTION, AND TESTING OF A NEW HIGH ACCURACY SPECTROPHOTOMETER		5. Publication Date June 1972	
		6. Performing Organization Code	
7. AUTHOR(S) K. D. Mielenz and K. L. Eckerle		8. Performing Organization	
9. PERFORMING ORGANIZATION NAME AND ADDRESS NATIONAL BUREAU OF STANDARDS DEPARTMENT OF COMMERCE WASHINGTON, D.C. 20234		10. Project/Task/Work Unit No.	
		11. Contract/Grant No.	
12. Sponsoring Organization Name and Address Same as No. 9.		13. Type of Report & Period Covered Final	
		14. Sponsoring Agency Code	

15. SUPPLEMENTARY NOTES

16. ABSTRACT (A 200-word or less factual summary of most significant information. If document includes a significant bibliography or literature survey, mention it here.)

A new spectrophotometer is described which has an accuracy of approximately 0.0001 transmittance units. The spectrophotometer utilizes a collimated beam in the sample area. This is accomplished by means of off-axis parabolic mirrors in the monochromator and sample compartment. Also, circular holes are used as entrance and exit apertures in the monochromator. All components of this spectrophotometer were chosen to achieve maximum accuracy. The result of this work is a "state of the art" instrument. The instrument was tested to evaluate its performance. Systematic errors such as detector non-linearity, stray radiant energy, and beam non-uniformity are measured. A correction for non-linearity of the photomultiplier and electronics is applied.

17. KEY WORDS (Alphabetical order, separated by semicolons) Beam non-uniformity; circular entrance and exit apertures; high accuracy spectrophotometer; linearity; parabolic mirrors; stray radiant energy; transmittance.

18. AVAILABILITY STATEMENT [X] UNLIMITED. [ ] FOR OFFICIAL DISTRIBUTION. DO NOT RELEASE TO NTIS.	19. SECURITY CLASS (THIS REPORT) UNCLASSIFIED	21. NO. OF PAGES 60
	20. SECURITY CLASS (THIS PAGE) UNCLASSIFIED	22. Price 60 cents

NBS TECHNICAL PUBLICATIONS

PERIODICALS

JOURNAL OF RESEARCH reports National Bureau of Standards research and development in physics, mathematics, and chemistry. Comprehensive scientific papers give complete details of the work, including laboratory data, experimental procedures, and theoretical and mathematical analyses. Illustrated with photographs, drawings, and charts. Includes listings of other NBS papers as issued.

Published in two sections, available separately:

• Physics and Chemistry

Papers of interest primarily to scientists working in these fields. This section covers a broad range of physical and chemical research, with major emphasis on standards of physical measurement, fundamental constants, and properties of matter. Issued six times a year. Annual subscription: Domestic, $9.50; $2.25 additional for foreign mailing.

• Mathematical Sciences

Studies and compilations designed mainly for the mathematician and theoretical physicist. Topics in mathematical statistics, theory of experiment design, numerical analysis, theoretical physics and chemistry, logical design and programming of computers and computer systems. Short numerical tables. Issued quarterly. Annual subscription: Domestic, $5.00; $1.25 additional for foreign mailing.

TECHNICAL NEWS BULLETIN

The best single source of information concerning the Bureau's measurement, research, developmental, co-operative, and publication activities, this monthly publication is designed for the industry-oriented individual whose daily work involves intimate contact with science and technology—*for engineers, chemists, physicists, research managers, product-development managers, and company executives.* Includes listing of all NBS papers as issued. Annual subscription: Domestic, $3.00; $1.00 additional for foreign mailing.

Bibliographic Subscription Services

The following current-awareness and literature-survey bibliographies are issued periodically by the Bureau: Cryogenic Data Center Current Awareness Service (weekly), Liquefied Natural Gas (quarterly), Superconducting Devices and Materials (quarterly), and Electromagnetic Metrology Current Awareness Service (monthly). Available only from NBS Boulder Laboratories. Ordering and cost information may be obtained from the Program Information Office, National Bureau of Standards, Boulder, Colorado 80302.

NONPERIODICALS

Applied Mathematics Series. Mathematical tables, manuals, and studies.

Building Science Series. Research results, test methods, and performance criteria of building materials, components, systems, and structures.

Handbooks. Recommended codes of engineering and industrial practice (including safety codes) developed in cooperation with interested industries, professional organizations, and regulatory bodies.

Special Publications. Proceedings of NBS conferences, bibliographies, annual reports, wall charts, pamphlets, etc.

Monographs. Major contributions to the technical literature on various subjects related to the Bureau's scientific and technical activities.

National Standard Reference Data Series. NSRDS provides quantitative data on the physical and chemical properties of materials, compiled from the world's literature and critically evaluated.

Product Standards. Provide requirements for sizes, types, quality, and methods for testing various industrial products. These standards are developed co-operatively with interested Government and industry groups and provide the basis for common understanding of product characteristics for both buyers and sellers. Their use is voluntary.

Technical Notes. This series consists of communications and reports (covering both other-agency and NBS-sponsored work) of limited or transitory interest.

Federal Information Processing Standards Publications. This series is the official publication within the Federal Government for information on standards adopted and promulgated under the Public Law 89–306, and Bureau of the Budget Circular A–86 entitled, Standardization of Data Elements and Codes in Data Systems.

Consumer Information Series. Practical information, based on NBS research and experience, covering areas of interest to the consumer. Easily understandable language and illustrations provide useful background knowledge for shopping in today's technological marketplace.

CATALOGS OF NBS PUBLICATIONS

NBS Special Publication 305, Publications of the NBS. 1966-1967. When ordering, include Catalog No. C13.10:305. Price $2.00; 50 cents additional for foreign mailing.

NBS Special Publication 305, Supplement 1, Publications of the NBS, 1968-1969. When ordering, include Catalog No. C13.10:305/Suppl. 1. Price $4.50; $1.25 additional for foreign mailing.

NBS Special Publication 305, Supplement 2, Publications of the NBS, 1970. When ordering, include Catalog No. C13.10:305/Suppl. 2. Price $3.25; 85 cents additional for foreign mailing.

Order NBS publications (except Bibliographic Subscription Services) from: Superintendent of Documents, Government Printing Office, Washington, D.C. 20402.